Inorganic Chemistry

Article

pubs.acs.org/IC

Oxidovanadium Catechol Complexes: Radical versus Non-Radical States and Redox Series

Suman Kundu,[†] Suvendu Maity,[†] Thomas Weyhermüller,[‡] and Prasanta Ghosh*[,†]

[†]Department of Chemistry, R. K. Mission Residential College, Narendrapur, Kolkata-103, India

[‡]Max-Planck Institute for Chemical Energy Conversion, Stiftstrasse 34-36, 45470 Muelheim an der Ruhr, Germany

Supporting Information

ABSTRACT: A new family of oxidovanadium complexes, $[(L_1^R)(VO)(L^{R'})]$ (R = H, R′ = H, **1**; R = H, R′ = -CMe_3, **2**; R = H, R′ = Me, **3**; R = -CMe_3, R′ = H, **4** and R = -CMe_3, R′ = -CMe_3, **5**), incorporating tridentate L_1^RH ligands (L_1^RH = 2,4-di-R-6-{(2-(pyridin-2-yl)hydrazono)methyl}phenol) and substituted catechols ($L^{R'}H_2$) was substantiated. The V−$O_{phenolato}$ (cis to V═O), V−O_{CAT} (cis to V═O) and V−O_{CAT} (trans to V═O) lengths span the ranges, 1.894(2)−1.910(2), 1.868(2)−1.887(2), and 2.120(2)−2.180(2) Å. The metrical oxidation states (MOS) of the catechols in **1**−**5** are fractional and vary from −1.43 to −1.60. The ^{51}V isotropic chemical shifts of solids and solutions of **1**−**5** are deshielded (^{51}V CP MAS: −19.8 to +248.6; DMSO-d_6: +173.9 to +414.55 ppm). The closed shell singlet (CSS) solutions of **1**−**5** are unstable due to open shell singlet (OSS) perturbations. The ground electronic states of **1**−**5** are defined by the resonance contribution of the catecholates ($L^{R'}{}_{CAT}{}^{2-}$) and $L^{R'}{}_{SQ}{}^{-\bullet}$ coordinated to the $[VO]^{3+}$ and $[VO]^{2+}$ ions. **1**−**5** are reversibly reducible by one electron at −(0.58−0.87) V, referenced vs ferrocenium/ferrocene, to VO^{2+} complexes, $[(L_1^{R-})(VO^{2+})(L^{R'}{}_{CAT}{}^{2-})]^-$ $[\mathbf{1}-\mathbf{5}]^-$. **1**−**5** display another quasi-reversible or irreversible reduction wave at −(0.80−1.32) V due to the formation of hydrazone anion radical ($L_1^{R2-\bullet}$) complexes, $[(L_1^{R2-\bullet})(VO^{2+})(L^{R'}{}_{CAT}{}^{2-})]^{2-}$, $[\mathbf{1}-\mathbf{5}]^{2-}$, with S = 1 authenticated by the unrestricted density functional theory (DFT) calculations on $\mathbf{1}^{2-}$ and $\mathbf{3}^{2-}$ ions. Frozen glasses electron paramagnetic resonance (EPR) spectra of $[\mathbf{1}-\mathbf{5}]^-$ ions [e.g., for **2**, $g_{\|}$ = 1.948, $g_{\perp}$ = 1.979, $A_{\|}$ = 164, $A_{\perp}$ = 60] affirmed that $[\mathbf{1}-\mathbf{5}]^-$ ions are the $[VO]^{2+}$ complexes of $L^{R'}{}_{CAT}{}^{2-}$. Spectro-electrochemical measurements and time-dependent DFT (TD DFT) calculations on **1**, **3**, $\mathbf{1}^-$, $\mathbf{3}^-$, and $\mathbf{1}^{2-}$ disclosed that the near infrared (NIR) absorption bands of **1**−**5** at 800 nm are due to the CSS-OSS metal to ligand charge transfer which are red-shifted in the solid state and disappear in $[\mathbf{1}-\mathbf{5}]^-$ and $[\mathbf{1}-\mathbf{5}]^{2-}$ ions.

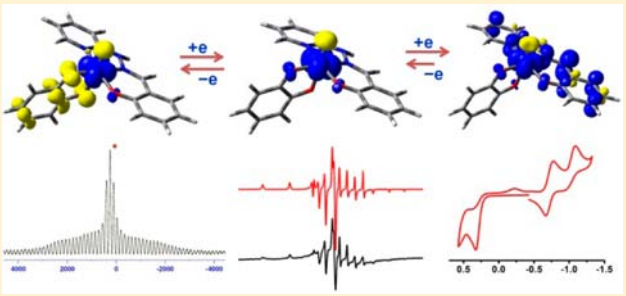

INTRODUCTION

One of the origins of the versatile biological activity of vanadium is the rich redox activities particularly of the oxidovanadium(IV/V) ion at biological pH.[1] In biology, the potential driven electron transfer occurs through the active-sites containing the redox active metal ions as well as through the redox-active organic fragments.[2] Thus, the possibility of developing new electronic states upon coordination of the redox active oxidovanadium(IV/V) ions to a redox active organic fragment is a subject of investigation. Common redox active ligands are catechols and *o*-aminophenols which participate in electron transfer reaction at lower potentials as illustrated in Scheme 1. Transition metal catechol and *o*-aminophenol complexes are numerous.[3] However catechol and aminophenol complexes of oxidovanadium ion are rare.[4]

Recently, we reported two families of *o*-iminobenzosemiquinone radical complexes of the oxidovanadium(IV) and their redox series.[5] In the present study, we have used catechols as redox active organic fragments which can sustain in malleable electronic states with the oxidovanadium ion as shown in Chart 1. We have been successful to isolate a new family of diamagnetic oxidovanadium complexes of type $[(L_1^R)(VO)(L^{R'})]$ (R = H, R′ = H, **1**; R = H, R′ = -CMe_3, **2**; R = H, R′ = Me, **3**; R = -CMe_3, R′ = H, **4** and R = -CMe_3, R′ = -CMe_3, **5**) incorporating substituted catechols ($L^{R'}H_2$) and a tridentate monodeprotonable NNO-donor ligand (L_1^RH). All the complexes are substantiated by elemental analyses, IR, Mass, UV−vis/NIR (solid state and CH_2Cl_2), ^1H NMR, ^{13}C NMR, ^{51}V NMR (CP MAS and DMSO-d_6), and single crystal X-ray structure determinations.

Elucidation of the electronic structure of **1**−**5** correlating the metrical parameters and spectral features is significant. The metrical parameters of the catecholato ligands, solutions and solid state ^{51}V NMR spectra and broken symmetry (BS) density functional theory (DFT) calculations authenticated that the catecholates in **1**−**5** are redox noninnocent toward the

Received: January 22, 2013
Published: June 20, 2013

   dx.doi.org/10.1021/ic400166z | *Inorg. Chem.* 2013, 52, 7417−7430

Scheme 1

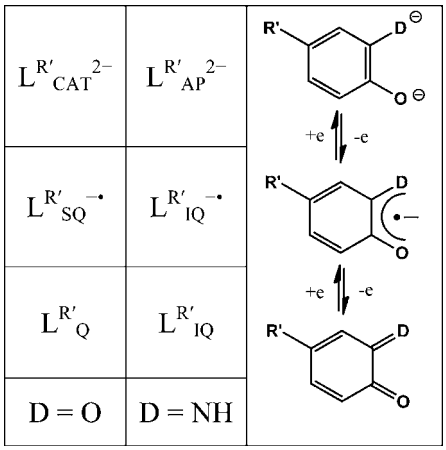

Chart 1

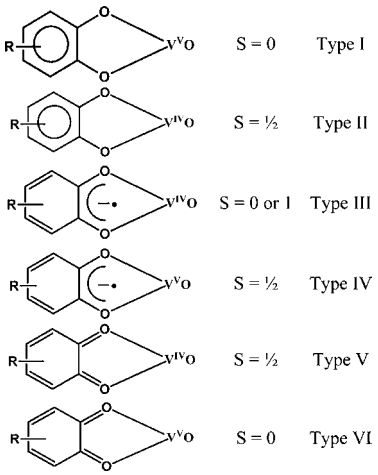

oxidovanadium ion. The metrical oxidation state (MOS) of the catecholates varies from −1.49 to −1.60. The ^{51}V isomer shifts span at −19.8 to +248.6 ppm in solid and +173.9 to +414.55 ppm in DMSO-d_6 which are unexpectedly more positive than those of the common VO^{3+} complexes. The closed shell singlet (CSS) solutions of **1**−**5** are unstable, while the BS (1,1) S = 0 solutions are stable (1,1 stands for one +1/2 spin and another −1/2 spin electrons). The experimental and quantum chemical observations inform that the electronic state of **1**−**5** cannot be explained only by the Type I state (Chart 2). The contribution of the diradical state to **1**−**5** where the *o*-benzosemiquinone radicals coordinate the oxidovanadium(IV) ion affording Type III electronic state as illustrated in Chart 2 has also been predicted. The solid state spectra are temperature dependent predicting an equilibrium between Type I and Type III electronic states.

1−**5** display two cathodic waves due to formation of $[(L_1{}^{R-})(VO^{2+})(L^{R'}_{CAT}{}^{2-})]^-$, $[\mathbf{1-5}]^-$ and hydrazone anion radical complexes $[(L_1{}^{R2-\bullet})(VO^{2+})(L^{R'}_{CAT}{}^{2-})]^{2-}$ of oxidovanadium(IV), with Type II (S = 1) electronic states. Formation of the hydrazone anion radical ($L_1{}^{R2-\bullet}$) with the oxidovanadium(IV) ion is an unprecedented observation. The results correlate well with the stabilization of the coupled diimine and azo anion radicals by the oxidovanadium(IV) ions, reported recently.[5b] The anodic waves of complexes **1**−**5** are irreversible prompting that *o*-benzoquinone ($L^{R'}_{Q}$) complexes with coordination Types V and VI (Chart 1) are unstable. The anionic complexes are analyzed by the electro- and spectro-electrochemical measurements, EPR spectra, DFT, and time-dependent DFT (TD DFT) calculations. The electronic structures, MOSs, ^{51}V NMR spectra, and redox series of **1**−**5** are compared with those of the *o*-iminobenzosemiquinone radical complexes of oxidovanadium(IV), $[(L_1{}^{R-})(VO^{2+})(L^{R'}_{IS}{}^{-\bullet})]$ (Chart 2) reported recently.[5a]

EXPERIMENTAL SECTION

Materials and Physical Measurements. Reagents or analytical grade materials were obtained from commercial suppliers and used without further purification. Spectroscopic grade solvents were used for spectroscopic and electrochemical measurements. The synthetic precursor, $VO(acac)_2$,[6] the tridentate ligands, 2-{(2-(pyridin-2-yl)-hydrazono)methyl}phenol ($L_1{}^{H}H$) and 2,4-di-*tert*-butyl-6-{(2-(pyridin-2-yl)hydrazono)methyl}phenol ($L_1{}^{t\text{-}Bu}H$) were prepared by the reported procedure.[7] $[(L_1{}^{H-})(VO^{2+})(L^{H}_{IS}{}^{-\bullet})]$ (**6**) and $[(L_1{}^{t\text{-}Bu-})(VO^{2+})(L^{H}_{IS}{}^{-\bullet})]$ (**7**) were prepared by the reported procedure.[5a] After evaporating MeOH solvents of the sample under high vacuum, elemental analyses and spectral measurements were performed. The C, H, and N content of the compounds were obtained from a Perkin-Elmer 2400 series II elemental analyzer. ESI mass spectrum was recorded on a micro mass Q-TOF mass spectrometer. Infrared spectra of the samples were measured from 4000 to 400 cm^{-1} with the KBr pellet at 298 K on a Perkin-Elmer Spectrum RX 1, FT-IR

Chart 2

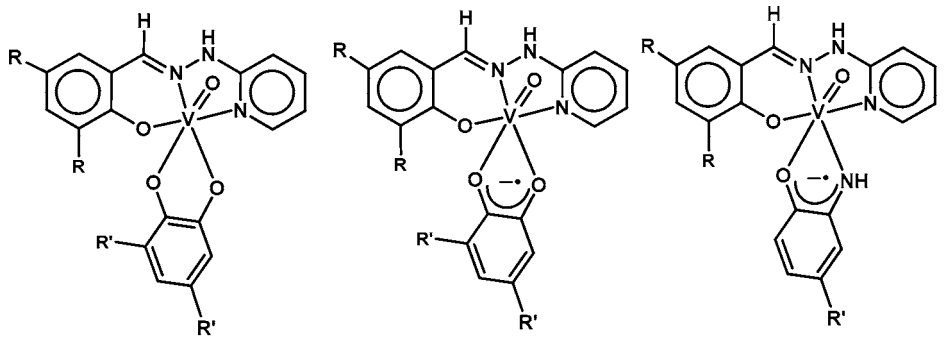

dx.doi.org/10.1021/ic400166z | Inorg. Chem. 2013, 52, 7417−7430

Spectrophotometer. ^{1}H NMR spectrum in $CDCl_3$ and DMSO-d_6 solvents were carried out on a Bruker DPX-300 MHz spectrometer with tetramethylsilane (TMS) as an internal reference. ^{51}V and ^{13}C NMR measurements were performed on a Bruker AV300 WB NMR Spectrometer using a standard 4 mm CP-MAS probe. Samples were packed in a 4 mm zirconium rotor and spun at 7 and 10 kHz. For ^{51}V CP MAS spectra V_2O_5 was used as an internal reference. 1 M solution of $NaVO_3$ at pH 12 was used as an internal reference for DMSO-d_6 solution spectra. For ^{13}C CP MAS spectra adamantane was used as an internal reference. Electronic absorption spectra in solutions and solids were carried out on a Perkin-Elmer Lambda 750 spectrophotometer in the range of 3300−175 nm. Solid state absorbance is recorded by the Kubelka−Munk function as $F(R) = (1 - R)^2/2R = k/s = Ac/s$, where, R = reflectance; k = absorption coefficient; s = scattering coefficient; c = concentration of the absorbing species; A = absorbance. Magnetic susceptibility at 298 K was measured on a Sherwood Magnetic Susceptibility Balance. The electro analytical instrument, BASi Epsilon-EC for cyclic voltammetric experiments in CH_2Cl_2 solutions containing 0.2 M tetrabutylammonium hexafluorophosphate as supporting electrolyte was used. The BASi platinum working electrode, platinum auxiliary electrode, Ag/AgCl reference electrode were used for the measurements. The redox potential data are referenced vs ferrocenium/ferrocene, Fc^+/Fc, couple. In all cases, the experiments were performed with the multiple scan rates to analyze the reversibility of the electron transfer waves. BASi SEC-C thin layer quartz glass spectro-electrochemical cell kit (light path length of 1 mm) with platinum gauze working electrode and SEC-C platinum counter electrode were used for spectro-electrochemistry measurements. The X-band EPR spectra were measured on a Bruker EMX spectrometer, where the microwave frequency was measured with a Hewlett-Packard 5246 L electronic counter.

Syntheses. *[(L_1^H)(VO)(L^H)] (**1**).* To 2-{(2-(pyridin-2-yl)hydrazono)-methyl}phenol (L_1^HH) (213 mg, 1.0 mmol) in a round-bottom flask methanol (25 mL) was added, and the resulting mixture was heated at 325 K to make a clear solution. The reaction mixture was cooled at 300 K and filtered. To this solution, a solution of $VO(acac)_2$ (267 mg, 1.0 mmol) in CH_2Cl_2 (5 mL) and methanol (5 mL) was added. The reaction mixture turned red. To this red solution, catechol, L^HH_2, (110 mg, 1.0 mmol) in methanol (10 mL) was added carefully, and the reaction mixture was allowed to evaporate slowly in air. After 2−3 days, black crystals of **1** separated out, which were collected upon filtration and dried in air. Yield: 220 mg (∼57% with respect to vanadium). Mass spectral data [electrospray ionization (ESI), positive ion, CH_3OH]: m/z 410.01 for [**1**+Na]$^+$, 388.04 for [**1**]$^+$. Anal. Calcd (%) for $C_{18}H_{14}N_3O_4V$: C, 55.83; H, 3.64; N, 10.85; Found: C, 55.58; H, 3.55; N, 10.52. ^{1}H NMR ($CDCl_3$, 300 MHz, 300 K): δ (ppm) = 14.45 (s, NH), 7.77 (d, 1H, J = 5.4 Hz), 7.37 (m, 2H), 7.00 (d, 3H, J = 9.0 Hz), 6.87 (t, 2H, J = 7.2 Hz), 6.68 (d, 2H, J = 7.5 Hz), 6.59 (m, 3H). (DMSO-d_6, 300 MHz, 300 K): δ (ppm) = 10.93 (s, NH), 8.68 (d, 2H), 7.81 (s, 1H), 7.58 (d, 2H), 6.93−6.65 (br, 8H). ^{13}C NMR (CP MAS, 75.47 MHz, 298 K): δ (ppm) = 164.78, 162.25, 158.88, 148.67, 146.23, 141.00, 138.64, 132.74, 130.88, 128.18, 117.89, 115.87, 114.35, 112.67, 105.75. IR/cm^{-1} (KBr): ν 3422 (m), 1630 (vs), 1598 (vs), 1543 (vs), 1485 (m), 1428 (s), 1430 (s) 1288 (vs), 1142 (s), 1110 (s), 959 (s), 754 (vs).

*[(L_1^H)(VO)($L^{t\text{-}Bu}$)] (**2**).* To 2-{(2-(pyridin-2-yl)hydrazono)methyl}-phenol (L_1^HH) (106 mg, 0.5 mmol) in a round-bottom flask methanol (20 mL) was added, and the resulting mixture was heated at 325 K to make a clear solution. The reaction mixture was cooled at 300 K and filtered. To this solution a solution of $VO(acac)_2$ (134 mg, 0.5 mmol) in CH_2Cl_2 (2 mL) and methanol (5 mL) was added. The reaction mixture turned red. To this red solution, 3,5-di-*tert*-butylcatechol, $L^{t\text{-}Bu}H_2$, (110 mg, 0.5 mmol), in methanol (5 mL) was added carefully, and the reaction mixture was allowed to evaporate slowly in air. After 2−3 days, black crystals of **2** separated out, which were collected upon filtration and dried in air. Yield: 150 mg (∼60% with respect to vanadium). Mass spectral data [electrospray ionization (ESI), positive ion, CH_3OH]: m/z 523.06 for [**2**+Na]$^+$, 500.08 for [**2**]$^+$. Anal. Calcd (%) for $C_{26}H_{30}N_3O_4V$: C, 62.52; H, 6.05; N, 8.41; Found: C, 62.38; H, 6.25; N, 8.53. ^{1}H NMR ($CDCl_3$, 300 MHz, 300 K): δ (ppm) = 14.43 (s, NH), 7.72 (d, 2H, J = 8.1 Hz), 7.35 (m, 3H), 7.02 (d, 2H, J = 12.6 Hz), 6.57 (t, 4H, J = 9.3 Hz), 1.32 (s, 9H), 1.24 (s, 9H). (DMSO-d_6, 300 MHz, 300 K): δ (ppm) = 12.67 (s, NH), 8.48 (s, 1H), 7.85 (s, 1H), 7.46 (m, 3H), 7.03−6.81 (br, 4H), 6.27 (d, 2H), 1.33 (s, 9H), 1.22 (s, 9H). ^{13}C NMR (CP MAS, 75.47 MHz, 298 K): δ (ppm) = 165.88, 160.99, 154.20, 151.29, 145.96, 141.83, 138.20, 134.56, 131.17, 129.47, 117.10, 113.95, 106.68, 33.22, 31.03, 28.37. IR/cm^{-1} (KBr): ν 1954 (vs), 1628 (vs), 1540 (vs), 1486 (s), 1430 (vs), 1336 (m), 1299 (s), 1230 (s), 1155 (m), 1105 (s), 994 (m), 961 (vs), 756 (s), 614 (m).

*[(L_1^H)(VO)(L^{Me})] (**3**).* To 2-{(2-(pyridin-2-yl)hydrazono)methyl}-phenol (L_1^HH) (213 mg, 1.0 mmol) in a round-bottom flask methanol (25 mL) was added, and the resulting mixture was heated at 325 K to make a clear solution. The reaction mixture was cooled at 300 K and filtered. To this solution a solution of $VO(acac)_2$ (267 mg, 1.0 mmol), in CH_2Cl_2 (5 mL) and methanol (5 mL) was added. The reaction mixture turned red. To this red solution, 4-methylcatechol, $L^{Me}H_2$, (124 mg, 1.0 mmol), in methanol (10 mL) was added carefully, and the reaction mixture was allowed to evaporate slowly in air. After 2−3 days, black crystalline compound of **3** separated out, which were collected upon filtration and dried in air. Yield: 225 mg (∼56% with respect to vanadium). Mass spectral data [electrospray ionization (ESI), positive ion, CH_3OH]: m/z 425.20 for [**3**+Na]$^+$, 402.2 for [**3**]$^+$. Anal. Calcd (%) for $C_{19}H_{16}N_3O_4V$: C, 56.87; H, 4.02; N, 10.47; Found: C, 56.78; H, 3.95; N, 10.42. ^{1}H NMR (DMSO-d_6, 300 MHz, 300 K): δ (ppm) = 10.56 (s, NH), 8.54 (s, 1H), 7.84−7.37 (br, 4H), 6.93−6.83 (br, 3H), 6.57−6.41 (m, 3H), 6.15 (s, 1H), 2.13 (s, -Me). ^{13}C NMR (CP MAS, 75.47 MHz, 298 K): δ (ppm) = 165.73, 161.70, 149.59, 146.18, 142.14, 137.80, 130.66, 127.56, 117.01, 110.80, 107.38, 20.48. IR/cm^{-1} (KBr): ν 3422 (m), 2362 (m), 1629 (vs), 1600 (m), 1541 (s), 1484 (s), 1429 (s), 1288 (m), 1261 (m), 1156 (m), 1105 (m), 951 (s), 757 (s), 612 (m).

*[($L_1^{t\text{-}Bu}$)(VO)(L^H)] (**4**).* To 2,4-di-*tert*-butyl-6-{(2-(pyridin-2-yl)-hydrazono)methyl}phenol ($L_1^{t\text{-}Bu}$H) (162 mg, 0.5 mmol) in a round-bottom flask methanol (20 mL) was added, and the resulting mixture was heated at 325 K to make a clear solution. The reaction mixture was cooled at 300 K and filtered. To this solution a solution of $VO(acac)_2$ (134 mg, 0.5 mmol) in CH_2Cl_2 (2 mL) and methanol (5 mL) was added. The reaction mixture turned red. To this red solution, catechol, L^HH_2 (55 mg, 0.5 mmol) in methanol (5 mL) was added carefully, and the reaction mixture was allowed to evaporate slowly in air. After 1−2 days, black crystals of **4** separated out, which were collected upon filtration and dried in air. Yield: 130 mg (∼52% with respect to vanadium). Mass spectral data [electrospray ionization (ESI), positive ion, CH_3OH]: m/z 522.08 for [**4**+Na]$^+$, 500.12 for [**4**]$^+$. Anal. Calcd (%) for $C_{26}H_{30}N_3O_4V$: C, 62.52; H, 6.05; N, 8.41; Found: C, 62.34; H, 5.93; N, 8.23. ^{1}H NMR ($CDCl_3$, 300 MHz, 300 K): δ (ppm) = 14.65 (s, NH), 7.76 (d, 2H, J = 7.5 Hz), 7.46 (d, 2H, J = 7.4 Hz), 6.94 (m, 2H), 6.73 (t, 2H, J = 9.1 Hz), 6.48 (s, 2H), 6.12 (s, 1H), 1.36 (s, 9H), 1.23 (s, 9H). (DMSO-d_6, 300 MHz, 300 K): δ (ppm) = 12.70 (s, NH), 9.80 (d, 1H), 8.74 (d, 1H), 7.89 (m, 2H), 7.41 (m, 2H), 7.01 (m, 2H), 6.73(s, 1H), 6.63 (s, 1H), 6.49 (s, 1H), 1.37 (s, 9H), 1.25 (s, 9H). ^{13}C NMR (CP MAS, 75.47 MHz, 298 K): δ (ppm) = 166.35, 159.21, 151.45, 145.25, 142.76, 139.35, 136.56, 132.83, 126.32, 124.45, 119.23, 117.32, 112.35, 107.38, 33.52, 31.35, 28.24, 26.38. IR/cm^{-1} (KBr): ν 2955 (s), 1627 (vs), 1550 (vs), 1485 (s), 1458 (m), 1429 (vs), 1314 (m), 1251 (s), 1137 (m), 959 (vs), 849 (m), 744 (m), 550 (m).

*[($L_1^{t\text{-}Bu}$)(VO)($L^{t\text{-}Bu}$)] (**5**).* To 2,4-di-*tert*-butyl-6-{(2-(pyridin-2-yl)-hydrazono)methyl}phenol ($L_1^{t\text{-}Bu}$H) (162 mg, 0.5 mmol) in a round-bottom flask methanol (20 mL) was added and the resulting mixture was heated at 325 K to make a clear solution. The reaction mixture was cooled at 300 K and filtered. To this solution a solution of $VO(acac)_2$ (134 mg, 0.5 mmol) in CH_2Cl_2 (2 mL) and methanol (5 mL) was added. The reaction mixture turned red. To this red solution, 3,5-di-*tert*-butylcatechol, $L^{t\text{-}Bu}H_2$, (110 mg, 0.5 mmol) in methanol (10 mL) was added carefully, and the reaction mixture allowed to evaporate slowly in air. After 1−2 days, black crystals of **5** separated out, which were collected upon filtration and dried in air. Yield: 186 mg (∼60% with respect to vanadium). Mass spectral data [electrospray

dx.doi.org/10.1021/ic400166z | Inorg. Chem. 2013, 52, 7417−7430

Table 1. Crystallographic Data for 1, 2, 4, and 5[a]

	1	2	4	5
formula	$C_{18}H_{14}N_3O_4V$	$C_{26}H_{30}N_3O_4V$	$C_{26}H_{30}N_3O_4V$	$C_{34}H_{46}N_3O_4V$
f_w	387.26	499.47	499.47	611.68
cryst color/system	black/monoclinic	black/monoclinic	black/trigonal	black/monoclinic
space group	$P2(1)/c$	$P2(1)/n$	$R\bar{3}$	$P2(1)/c$
a (Å)	8.0221(4)	13.9332(8)	38.113(4)	14.305(2)
b (Å)	10.1413(7)	9.8988(5)	38.113(4)	17.230(2)
c (Å)	20.3138(9)	18.1730(6)	10.0207(11)	13.792(2)
α (deg)	90	90	90	90
β (deg)	97.794(4)	96.545(4)	90	96.046(11)
γ (deg)	90	90	120	90
V (Å)	1637.35(16)	2490.1(2)	12606(2)	3380.5(8)
Z	4	4	18	4
T (K)	100(2)	100(2)	100(2)	100(2)
μ (mm^{-1})	0.636	0.435	0.386	0.332
ρ calcd (g cm^{-3})	1.571	1.332	1.184	1.202
refl. collected ($2\Theta_{max}$)	71.98	66.32	66.52	66.16
unique refl.	34193	69606	152632	93444
ref ($I > 2\sigma$)	6993	7940	9287	9193
F(000)	792	1048	4716	1304
no. of params/restr.	235/0	316/1	316/1	394/0
λ (Å /μ)	0.71073	0.71073	0.71073	0.71073
R1[b]/goodness of fit[c]	0.0281/1.060	0.0387/1.140	0.0329/1.056	0.0381/1.018
wR2[d] [$I > 2\sigma$ (I)]	0.0785	0.0977	0.0901	0.0825
residual density (e $Å^{-3}$)	0.597/−0.593	0.495/−0.496	0.518/−0.277	0.479/−0.437

[a]Observation criterion: $I > 2\sigma(I)$. [b]$R1 = \sum||F_o| - |F_c||/\sum|F_o|$. [c]$GOF = \{\sum[w(F_o^2 - F_c^2)^2]/(n-p)\}^{1/2}$. [d]$wR2 = \{\sum[w(F_o^2 - F_c^2)^2]/\sum[w(F_o^2)^2]\}^{1/2}$ where $w = 1/[\sigma^2(F_o^2) + (aP)^2 + bP]$, $P = (F_o^2 + 2F_c^2)/3$.

ionization (ESI), positive ion, CH_3OH]: m/z 634.44 for [**5**+Na]$^+$, 612.46 for [**5**]$^+$. Anal. Calcd (%) for $C_{34}H_{46}N_3O_4V$: C, 66.76; H, 7.58; N, 6.87; Found: C, 66.64; H, 7.39; N, 6.83. ^{1}H NMR ($CDCl_3$, 300 MHz, 300 K): δ (ppm) = 14.69 (s, NH), 7.69 (d, 1H, J = 7.6 Hz), 7.44 (s, 1H), 7.34 (s, 1H), 6.59 (d, 1H, J = 7.5 Hz), 6.50 (s, 1H), 6.46 (m, 2H), 6.14 (s, 1H), 6.10 (s, 1H), 1.33 (s, 18H), 1.30 (s, 9H), 1.25 (s, 9H). (DMSO-d_6, 300 MHz, 300 K): δ (ppm) = 12.57 (s, NH), 8.46 (s, 1H), 7.84 (t, 1H), 7.57 (s, 1H), 7.36 (m, 2H), 7.01 (d, 2H), 6.26 (s, 1H), 6.09 (s, 1H), 1.39 (s, 9H), 1.31 (s, 9H), 1.25 (s, 9H), 1.18 (s, 9H). ^{13}C NMR (CP MAS, 75.47 MHz, 298 K): δ (ppm) = 163.56, 159.83, 152.39, 147.42, 140.90, 138.11, 134.39, 131.90, 129.11, 125.07, 115.45, 113.90, 111.42, 106.14, 33.17, 31.91, 29.75, 28.48. IR/cm^{-1} (KBr): ν 2953 (vs), 1626 (vs), 1582 (s), 1550 (s), 1483 (s), 1433 (vs), 1359 (s), 1230 (s), 1227 (s), 1197 (s), 994 (m), 956 (vs), 846 (m), 760 (m), 540 (m).

Single Crystal X-ray Structure Determinations of the Complexes. Dark single crystals of **1**, **2**, **4**, and **5** were picked up with nylon loops and were mounted on a Bruker APEX-II CCD diffractometer (at 100 K) equipped with a Mo-target rotating-anode X-ray source and a graphite monochromator (Mo−Kα, λ = 0.71073 Å). Final cell constants were obtained from least-squares fits of all measured reflections. Intensity data were corrected for absorption using intensities of redundant reflections. The structures were readily solved by direct methods and subsequent difference Fourier techniques. The crystallographic data of **1**, **2**, **4**, and **5** have been listed in Table 1. The Siemens SHELXS-97[8] software package was used for solution, and SHELXL-97[8] was used for the refinement. All non-hydrogen atoms were refined anisotropically. Hydrogen atoms were placed at the calculated positions and refined as riding atoms with isotropic displacement parameters. The level **A**-alert of the structure of **4** is about solvent voids. The compound can be considered a MOF with hexagonal channels along the c-axis which are not filled with solvent anymore. The packing of complex molecules is so stable that the structure does not collapse and shows such voids.

Density Functional Theory (DFT) Calculations. All calculations reported in this Article were done with the Gaussian 03W[9] program package supported by GaussView 4.1. The DFT[10] and TD DFT[11] calculations were performed at the level of Becke three parameter hybrid functional with the nonlocal correlation functional of Lee−Yang−Parr (B3LYP)[12] with the nonlocal correlation provided by Perdew/Wang 91 (B3PW91)[13] and with a hybrid exchange-correlation functional, PBE1PBE.[14] Gas-phase geometries of complexes, **1** and **3** were optimized with Pualy's Direct Inversion[15] in the Iterative Subspace (DIIS), "tight" convergent SCF procedure[16] ignoring symmetry, with singlet and triplet spin states with all three functionals for comparison. Stabilities of all singlet solutions were checked, and the unstable solutions were reoptimized. Singlet solutions of all these species are unstable, but the BS (1,1) solutions, converging to M_s = 0 solutions, are stable indicating that the open shell electronic structure is correlating bond parameters well. Gas phase geometries of the monoanions (**1**$^-$ and **3**$^-$) with doublet spin state and dianions (**1**$^{2-}$ and **3**$^{2-}$) with singlet and triplet spin states were optimized using only a hybrid functional (B3LYP). Similarly, the gas phase geometry of [(L_1^{R-})(VO)(L_{OO}^{2-})] (**8**) with singlet spin state was optimized using B3LYP functional to investigate the stability of the solution that incorporates redox innocent ligand (L_{OO}^{2-} = dianionic(1*R*,2*S*)-cyclohexane-1,2-bis(olate). All the calculations were performed with a LANL2DZ basis set,[17] along with the corresponding effective core potential (ECP) for vanadium, 6-31G(d, p)[18] basis set for C, O, N atoms, and 6-31G[19] for H atoms. BS DFT calculations were performed using the quadratic convergent self-consistent field (SCF) method. The 60 lowest singlet excitation energies on the optimized geometries of **1** and **3** with singlet spin state were calculated by the TD DFT method.[11] The ^{1}H NMR, ^{13}C and ^{51}V NMR parameters were calculated at the DFT level at both the optimized and the X-ray geometries of **1**. For these calculations, **1** was optimized using the 6-311++G(d, p)[20] basis set with the B3LYP functional. The ^{51}V chemical shifts are referenced with respect to $VOCl_3$. The $VOCl_3$ was optimized using the same basis sets.

RESULTS

Syntheses and Characterization. The oxidovanadium complexes of substituted catechols ($L^{R'}H_2$), established in this

dx.doi.org/10.1021/ic400166z | Inorg. Chem. 2013, 52, 7417−7430

work are listed in Chart 3. The tridentate NNO-donor ligands (L_1^RH) were prepared by the reported procedures (R = H,

Chart 3. $L^{R'}{}_{CAT}{}^{2-}$ and $L^{R'}{}_{SQ}$ Complexes of Oxidovanadium(IV/V) Ion (*t*-Bu refers to -CMe_3 group)

R	R′	$[(L_1^{R-})(VO)(L^{R})]$	$[(L_1^{R-})(V^{IV}O)(L^{R}{}_{CAT}{}^{2-})]^-$	$[(L_1^{R2-\bullet})(V^{IV}O)(L^{R}{}_{CAT}{}^{2-})]^{2-}$
H	H	**1**	$[\mathbf{1}]^-$	$[\mathbf{1}]^{2-}$
H	*t*-Bu	**2**	$[\mathbf{2}]^-$	$[\mathbf{2}]^{2-}$
H	Me	**3**	$[\mathbf{3}]^-$	$[\mathbf{3}]^{2-}$
t-Bu	H	**4**	$[\mathbf{4}]^-$	$[\mathbf{4}]^{2-}$
t-Bu	*t*-Bu	**5**	$[\mathbf{5}]^-$	$[\mathbf{5}]^{2-}$

L_1^HH = 2-{(2-(pyridin-2-yl)hydrazono)methyl}phenol; R = *t*-Bu, $L_1^{t\text{-}Bu}H$ = 2,4-di-*tert*-butyl-6-{(2-(pyridin-2-yl)hydrazono)-methyl}phenol).[7] Complexes **1**−**5** were characterized by elemental analyses, Mass spectral data, IR, and ^1H, ^{13}C and ^{51}V NMR spectra. The data are listed in the Experimental Section. In complexes **1**−**5**, the V═O stretching vibrations appear respectively at 959, 961, 951, 959, and 956 cm^{-1}.

UV−vis/NIR absorption spectra of CH_2Cl_2 solutions of **1**−**5** at 298 K were illustrated in Figure 1, and the spectral data are

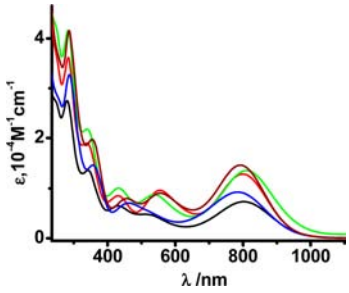

Figure 1. Electronic spectra of **1** (black), **2** (red), **3** (green), **4** (blue), and **5** (olive) in CH_2Cl_2 at 298 K.

Table 2. Electronic Absorption Spectral Data of [1−5], [1−5]$^-$, and [1−5]$^{2-}$ in CH_2Cl_2 at 298 K

comp	λ_{max} (nm) (ε, 10^{-4} M^{-1} cm^{-1})
1	802 (0.73), 530 (0.48), 430 (0.65), 342 (1.36), 280 (2.75)
$\mathbf{1}^-$	808 (0.21), 525 (0.12), 411 (1.08), 336 (1.40)
$\mathbf{1}^{2-}$	825 (0.02)^{sh}, 410 (0.54), 341 (2.14)
2	801 (1.29), 554 (0.97), 430 (0.85), 338 (1.89), 284 (3.61)
$\mathbf{2}^-$	803 (0.55), 550 (0.50), 411 (1.57), 335 (2.24)
$\mathbf{2}^{2-}$	815 (0.02)^{sh}, 397 (0.73), 328 (2.91)
3	811 (1.37), 537 (0.88), 432 (1.00), 341 (2.18), 284 (4.17)
$\mathbf{3}^-$	814 (0.72), 538 (0.51), 412 (2.11), 337 (2.79)
$\mathbf{3}^{2-}$	823 (0.03)^{sh}, 409 (1.03), 338 (4.06)
4	786 (0.94), 462 (0.70), 357 (1.47), 286 (3.26)
$\mathbf{4}^-$	789 (0.44), 516 (0.31), 428 (0.94), 346 (1.65)
$\mathbf{4}^{2-}$	615 (0.06), 425 (0.55), 355 (2.17)
5	794 (1.47), 556 (0.91), 455 (0.80), 356 (1.98), 246 (4.14)
$\mathbf{5}^-$	715 (0.60), 426 (1.14), 352 (2.06)
$\mathbf{5}^{2-}$	805 (0.07), 425 (0.45), 344 (2.56)

summarized in Table 2. The characteristic absorptions are similar for all five complexes with a lower energy absorption band at around 800 nm which disappears upon reduction. The electronic spectral features of the $[\mathbf{1}-\mathbf{5}]^-$ and $[\mathbf{1}-\mathbf{5}]^{2-}$ ions were recorded by coulometric and spectro-electrochemical measurements (vide infra). Data are listed in Table 2. The origins of the absorptions of **1**−**5** and the reduced analogues were investigated by TD DFT calculations (vide infra) on **1**, **3**, $\mathbf{1}^-$, $\mathbf{3}^-$, and $\mathbf{1}^{2-}$.

Single Crystal X-ray Structures. Molecular geometries of the complexes were confirmed by the single crystal X-ray structure determinations of **1**, **2**, **4**, and **5**. The observed bond parameters are very significant to the assignment of the oxidation level of the catechol ligands ($L^{R'}H_2$) as well as of the [VO] core. For higher precision of the bond parameters all the crystallographic data were collected at 100 K. The V−$O_{phenolato}$ bonds cis to V═O are significant to analyze the oxidation level of oxidovanadium ion.[5]

1 crystallizes in the $P2_1/c$ space group. Molecular geometry of **1** in crystals with the atom labeling scheme is shown in the panel (a) of Figure 2. Significant bond parameters are

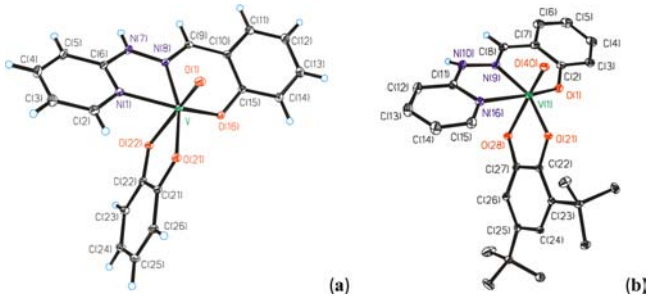

Figure 2. Molecular geometries of (a) **1** and (b) **2** in crystals (50% thermal ellipsoids and hydrogen atoms are omitted for clarity).

summarized in Table 3. The monoanionic tridentate L_1^{H-} ligand spans the meridional sites. The V−$O_{phenolato}$ bonds, V−O(16) and V−O(22), cis to the V═O bond, are 1.8946(6) and 1.8681(6) Å which are shorter than a V^{IV}−$O_{phenolato}$ (cis) length but longer than a V^{V}−$O_{phenolato}$ (cis) length.[5] V−O(21) is longer due to the trans influence of the V═O bond. Two C−O lengths are significantly different and the average lengths are longer than C−O_{SQ} and shorter than C−O_{CAT} lengths.

2 crystallizes in $P2_1/n$ space group. An ORTEP plot of **2** and the atom-labeling scheme are illustrated in the panel (b) of Figure 2. Supporting Information, Table S1 summarizes the significant bond parameters. Similar to **1**, the monoanionic tridentate L_1^{H-} ligand spans the meridional sites. The V−$O_{phenolato}$ bonds, V−O(1) and V−O(21), cis to the V═O bond, are 1.9097(10) and 1.8758(8) Å which are shorter than a V^{IV}−$O_{phenolato}$ (cis)[5] length but longer than a V^{V}−$O_{phenolato}$ (cis) length.[5] V−O(28) is longer due to trans influence of the V═O bond. Two C−O lengths are unequal, and the trend does not support the coordination of a pure catecholate ligand ($L^{t\text{-}Bu}{}_{CAT}{}^{2-}$) to the oxidovanadium(V) or a benzosemiquinone ligand ($L^{t\text{-}Bu}{}_{SQ}{}^{-\bullet}$) to the oxidovanadium(IV).

4 and **5** crystallize respectively in $R\bar{3}$ and $P2_1/c$ space groups. Molecular geometries of **4** and **5** in crystals with the atom labeling scheme are depicted in Supporting Information, Figure S1. Significant bond parameters are summarized in Supporting Information, Tables S2 and S3. The V−$O_{phenolato}$ bonds of **4**, V−O(11) and V−O(48), cis to the V═O bond, are 1.8818(7) and 1.8817(7) Å. Similarly, the V−$O_{phenolato}$ bonds of **5**, V−O(1) and V−O(31), cis to the V═O bond, are 1.8939(8) and 1.8870(8) Å. These lengths are comparable to those of **1** and **2** complexes.

Two V−O and C−O lengths of the OO-chelate are significantly different. V−O length trans to V═O bond is longer due to the trans influence of the V═O bond. The trend

dx.doi.org/10.1021/ic400166z | Inorg. Chem. 2013, 52, 7417−7430

Table 3. Selected Experimental Bond Lengths (Å) and Angles (deg) of 1 and Calculated Parameters of 1, 1^+, 1^-, and 1^{2-}, Using B3LYP, B3PW91, and PBE1PBE Functionals

		calcd						
	exptl	1				1^+	1^-	1^{2-}
	1	BS(1,1) M_s = 0[a]	BS(1,1) M_s = 0[b]	BS(1,1) M_s = 0[c]	M_s = 1[a]	M_s= 1/2[a]	M_s= 1/2[a]	M_s = 1[a]
V−O(1)	1.606(2)	1.5958	1.5906	1.5847	1.593	1.574	1.6200	1.624
V−O(16)	1.895(2)	1.8807	1.8688	1.8618	1.923	1.815	1.9879	1.979
V−O(21)	2.162(2)	2.1450	2.1207	2.1096	2.322	2.341	2.1088	2.186
V−O(22)	1.868(2)	1.8386	1.8283	1.8201	2.009	1.865	1.9339	1.995
V−N(1)	2.113(2)	2.1280	2.1108	2.1041	2.154	2.119	2.1937	2.176
V−N(8)	2.104(2)	2.1394	2.1265	2.1206	2.081	2.106	2.1207	2.069
O(21)−C(21)	1.317(2)	1.2970	1.2957	1.2944	1.272	1.258	1.3194	1.305
O(22)−C(22)	1.335(2)	1.3319	1.3304	1.3298	1.292	1.309	1.3365	1.325
O(16)−C(15)	1.330(2)	1.3093	1.3051	1.3030	1.305	1.335	1.2879	1.302
C(22)−C(23)	1.404(2)	1.4028	1.3995	1.3970	1.417	1.402	1.3978	1.400
C(23)−C(24)	1.385(2)	1.3895	1.3888	1.3875	1.381	1.386	1.4060	1.412
C(24)−C(25)	1.405(2)	1.4126	1.4088	1.4064	1.427	1.435	1.3959	1.393
C(25)−C(26)	1.391(2)	1.3884	1.3877	1.3864	1.374	1.369	1.4042	1.409
C(26)−C(21)	1.408(2)	1.4158	1.4122	1.4098	1.432	1.440	1.4047	1.409
C(21)−C(22)	1.420(2)	1.4335	1.4289	1.4256	1.474	1.476	1.4350	1.447
N(7)−N(8)	1.375(2)	1.3783	1.3667	1.3636	1.381	1.373	1.3815	1.385
N(8)−C(9)	1.297(2)	1.299	1.298	1.295	1.299	1.302	1.294	1.323
O(1)−V−O(21)	172.09(3)	170.09	169.98	170.16	171.25	172.51	168.77	169.95
O(1)−V−O(22)	95.48(3)	96.87	96.75	96.98	101.64	100.98	102.79	96.46
O(21)−V−O(22)	77.78(2)	78.28	78.65	78.92	74.98	75.27	79.50	76.77
O(1)−V−O(16)	100.72(3)	101.91	101.65	101.59	104.31	103.40	99.76	100.03

[a]B3LYP. [b]B3PW91. [c]PBE1PBE.

Table 4. MOS Analyses of 1−5[a]

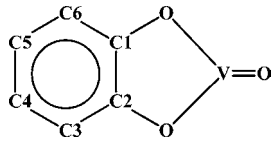

comp	C−O	C1−C2	C2−C3 C6−C1	C3−C4 C5−C6	C4−C5	esd	Type I (%)	Type III (%)
exptl, **1**	1.3261(9)	1.4200(10)	1.4063(10)	1.3879(12)	1.4051(13)			
calcd, MOS = −1.60	***1.3274***	***1.4235***	***1.4045***	***1.3823***	***1.4015***	***0.036***	***60***	***40***
DFT calcd, **1**	1.3144	1.4335	1.4093	1.3889	1.4126			
calcd, MOS = −1.43	***1.3156***	***1.4323***	***1.4104***	***1.3784***	***1.4094***	***0.051***	***43***	***57***
exptl, **2**	1.3248(14)	1.4236(16)	1.4140(15)	1.387(16)	1.4199(16)			
calcd, MOS = −1.49	***1.3198***	***1.4291***	***1.4083***	***1.3798***	***1.4066***	***0.082***	***49***	***51***
exptl, **4**	1.3227(11)	1.4266(12)	1.4065(12)	1.3871(14)	1.4049(15)			
calcd, MOS = −1.56	***1.3246***	***1.4255***	***1.4059***	***1.3814***	***1.4033***	***0.028***	***56***	***44***
exptl, **5**	1.3296(13)	1.4171(15)	1.4113(14)	1.3885(16)	1.4164(16)			
calcd, MOS = −1.57	***1.3253***	***1.4250***	***1.4056***	***1.3816***	***1.4029***	***0.087***	***57***	***43***

[a]Using the procedure of reference 21.

of bond parameters of the catechol fragments in all four structures is very similar as illustrated in Supporting Information, Chart S1. The features of C−O and C−C lengths of the OO-chelate do not support a pure dianionic $L^{R'}{}_{CAT}{}^{2-}$ chelate or a monoanionic $L^{R}{}_{SQ}{}^{-\bullet}$ radical chelate coordinated to the oxidovanadium (IV/V) ions. The average C−O lengths in **1**, **2**, **4**, and **5** are 1.3261(9), 1.3248(14), 1.3227(11), and 1.3296 Å, respectively, which are shorter than those of a pure dianionic catecholate chelate with the C−O length, 1.35 ± 1 Å. The C1−C6 lengths are longer than an aromatic C−C length. A quinoidal distortion of the phenyl ring is observed in all cases. C2−C3 and C4−C5 lengths are shorter than C1−C2, C3−C4, and C5−C6 lengths (Supporting Information, Chart S1). These parameters strongly suggest the partial oxidation of catecholato ligands to the *o*-benzosemiquinone radicals and correlate well with the contribution of the Types I and III states to the ground electronic state of complexes **1**−**5** as depicted in Chart 2. In the lattice of all the complexes, strong intermolecular H-bonding interactions (N---O distances: 2.691 Å in **1**, 2.679 Å in **2**, 2.649 Å in **4** and 2.646 Å in **5**) between the catecholato oxygen and the −NH group as depicted in Supporting Information, Figure S2 has been observed.

Metrical Oxidation State (MOS). Metrical oxidation states (MOS) of the redox noninnocent catecholates in **1**−**5** are important parameters to analyze the electronic state of their complexes. The MOS of the catecholates of **1**−**5** have been

dx.doi.org/10.1021/ic400166z | Inorg. Chem. 2013, 52, 7417−7430

calculated by a reported procedure using X-ray structural and theoretical bond parameters.[21] Data are summarized in Table 4. Ignoring completely the existence of the benzoquinone state in **1**−**5**, the fractional MOS are correlated by the presence of $L^{R'}{}_{SQ}{}^{-\bullet}$ and $L^{R'}{}_{CAT}{}^{2-}$ states.[22] The calculated percentage contribution of $L^{R'}{}_{SQ}{}^{-\bullet}$ and $L^{R'}{}_{CAT}{}^{2-}$ in **1**−**5** are also listed in Table 4.

^{1}H and ^{13}C NMR Spectra. ^{1}H NMR spectra in $CDCl_3$, DMSO-d_6 and solid state ^{13}C NMR spectra of **1**−**5** were recorded. Data are summarized in the Experimental Section. Unequivocal assignments of the protons and carbons in closely spaced spectra are difficult. Comparing with the experimental ^{1}H NMR and ^{13}C NMR spectra of the free ligands ($L_1{}^RH$) the significant protons and carbons particularly of the catechol ligands of **1**−**5** have been assigned. To support the assignments, ^{1}H NMR and ^{13}C NMR spectra on the gas phase optimized geometry of **1** have been calculated at the B3LYP/DFT level. The calculated data are listed in Chart 4. The calculations show

Chart 4. Calculated ^{1}H and ^{13}C NMR Data of 1

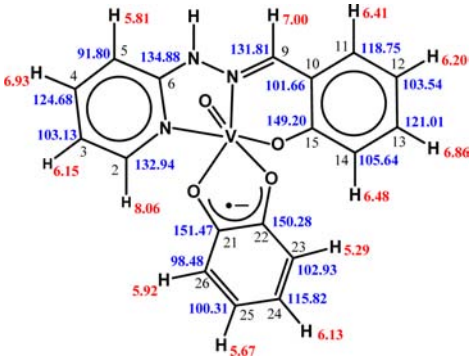

that the four C−H protons (C21−C26) of the catechol ring as depicted in Chart 4 and one of the pyridine C−H protons (C5) are significantly shielded. The calculated shielding range of these protons is 5.30−6.0 ppm. It is observed that the protons of the free $L_1{}^RH$ ligands do not span below 6.8 ppm. Thus, the resonances at less than 6.8 ppm have been assigned to catechol C−H protons (C23−H, C24−H, C25−H, and C26−H) and one pyridine C−H proton (C5−H, Chart 4). They appear at: **1**, 6.68 (d, 2H, J = 7.5 Hz), 6.59 (m, 3H); **4**, 6.73 (t, 2H, J = 9.1 Hz), 6.48 (s, 2H), 6.12 (s, 1H); **5**, 6.14 (s, 1H), 6.10 (s, 1H) in $CDCl_3$ solvent. It correlates well with the oxidation of the catechols decreasing the paramagnetic ring current at the periphery. Similarly, the C−H carbon atoms (C23−C26) of the catechol ring are shielded resonating at 120−105 ppm, while the carbon atoms, C21 and C22, of the OO-chelate including the phenolato carbon (C15) and the imine carbon (C9) atoms are deshielded. In ^{13}C NMR spectra, they are assigned to 166.35−145.25 ppm. The deshielding of the C−O carbon atoms during the conversions of the hydroquinone to quinone is reported. The C−O carbon atoms of the naphthohydroquinone appear at 143.6, which are shifted to 184.7 in naphthoquinone.[23]

^{51}V NMR Spectra. Electronic structure of the oxidovanadium complexes incorporating redox noninnocent catechols were analyzed by the chemical shift, the electric field gradient (EFG), and chemical shift anisotropy (CSA) tensor parameters.[4b,c,24] ^{51}V quadrupole coupling constants of the oxidovanadium complexes incorporating redox noninnocent ligands are surprisingly small, compared to the common oxidovanadium(V) complexes. CP MAS and solution ^{51}V NMR spectra of **1**−**5** were recorded. The relevant spectra are shown in Figure 3 and Supporting Information, Figure S3. The data are summarized in Table 5.

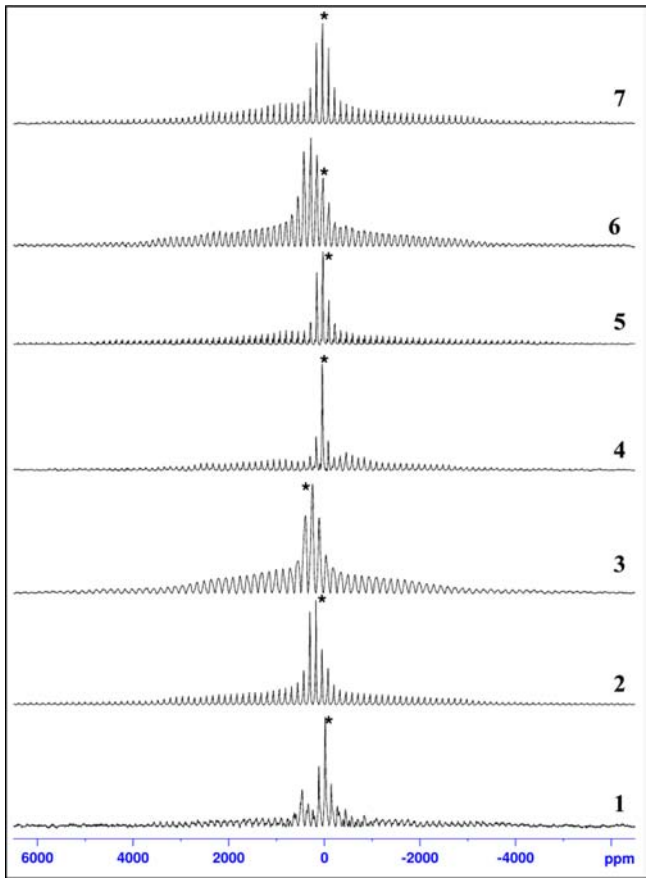

Figure 3. 78.94 MHz ^{51}V CP MAS spectra of **1**−**7** at 10 kHz spinning (Isotropic peaks are marked with *).

Table 5. Experimental and Calculated Isotropic Chemical Shifts of ^{51}V Nuclei in 1−7

	^{51}V δ_{iso} (ppm)		
comp	CP MAS[a]	DMSO-d_6[b]	calcd
1	−19.8	+243.21	+65.1[c], −31.3[d]
2	+173.6	+414.55	
3	+248.6	+352.85	
4	+43.9	+173.93	
5	+29.7	+345.35	
6	+43.9	+190.49	
7	+36.8	+153.16	

[a]Isotropic peak of V_2O_5 taken at −610 δ as internal reference. [b]1 M solution of $NaVO_3$ at pH 12: $VO_4{}^{3-}$ at −536 δ as internal reference. [c]DFT on optimized geometry. [d]DFT on X-ray geometry.

In CP MAS spectra, ^{51}V isotropic chemical shifts of **1**−**5** span the range −19.8 to +248.6 ppm, while in solutions the resonances are deshielded to +173.9 to +414.55 ppm. The isotropic chemical shift parameters correlate well with the reported parameters of similar type of complexes.[4b,c,24] In **1**−**5**, the ^{51}V nuclei are deshielded compared to common $[VO]^{3+}$ complexes. The quantum chemical calculations have repro-

dx.doi.org/10.1021/ic400166z | Inorg. Chem. 2013, 52, 7417−7430

duced the similar parameters. The chemical shift of ^{51}V nucleus has been calculated on the gas phase optimized and X-ray geometries of **1**. The calculated shifts are listed in Table 5. The calculated shielding parameters are comparable to those obtained from the CP MAS ^{51}V NMR spectra of **1**. In solutions, the nuclei are more deshielded. CP MAS ^{51}V NMR spectra of $[(L_1^{H-})(VO^{2+})(L^{H}_{IS}{}^{-\bullet})]$ (**6**) and $[(L_1^{t\text{-}Bu-})(VO^{2+})(L^{H}_{IS}{}^{-\bullet})]$ (**7**) containing the oxidovanadium(IV) ion coupled to *o*-iminobenzosemiquinone radical ($L^{H}_{IS}{}^{-\bullet}$, Scheme 1) were recorded (Figure 3) for comparison. The ^{51}V isotropic chemical shifts of **6** and **7** are also comparable to **1**−**5**. The deshielding effect of ^{51}V nuclei can be explained by the redox noninnocence of the catechols producing $L^{R'}{}_{SQ}{}^{-\bullet}$ coordinated to oxidovanadium(IV) ion.

Redox Series and EPR Spectra. **1**−**5** are redox-active. To analyze the stabilities and the electron transfer series of the complexes, redox-activities of complexes **1**−**5** were investigated at 298 K by cyclic voltammetry in CH_2Cl_2 containing 0.2 M tetrabutylammonium hexafluorophosphate as supporting electrolytes. The experiments were performed with different scan rates. The redox potential data were referenced vs ferrocenium/ferrocene, Fc^+/Fc, couple and summarized in Table 6. The

Table 6. Redox Potential of 1−5 Determined by Cyclic Voltammetry in CH_2Cl_2 (0.2 M $[N(n\text{-}Bu)_4]PF_6$) at 298 K

comp	E_p^1 (V)[a]	$E_{1/2}^2$ (V) (ΔE[b], mV)	E_p^3 (V)[c]
1	0.42	−0.58(84)	−0.84[−0.80(97)][d]
2	0.32	−0.72(111)	−1.08[−1.02(120)][d]
3	0.37	−0.62(96)	−0.89
4	0.45	−0.70(117)	−1.06
5	0.35	−0.87(217)	−1.32

[a]Anodic peak potential. [b]Peak-to-peak separation. [c]Cathodic peak potential. [d]$E_{1/2}$ with peak-to-peak separation in mV.

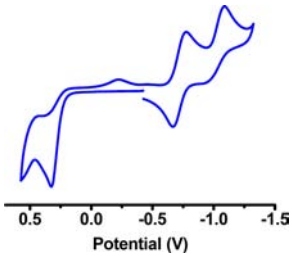

Figure 4. Cyclic voltammogram of **2** in CH_2Cl_2 at 298 K. Conditions: 0.2 M $[N(n\text{-}Bu)_4]PF_6$ supporting electrolyte; scan rate, 100 mV s^{-1}; platinum working electrode. Potential data referenced vs Fc^+/Fc, couple.

cyclic voltammogram of **2** is shown in Figure 4. The cyclic voltammograms of **1**, **3**, **4**, and **5** are shown in Supporting Information, Figure S4. The cathodic waves of **1**−**5** at −(0.58−0.87) V ($E_{1/2}^2$) are reversible. The second cathodic waves are not reversible. They are quasi-reversible in cases of **1** and **2** while those of **3**−**5** are irreversible (E_p^3, Table 6). EPR spectra and DFT calculations authenticated that $E_{1/2}^2$ is due to the formation of $[(L^{R'}{}_{CAT}{}^{2-})(V^{IV}O)]$ complexes while the E_p^3 is due to the formation of hydrazone anion radical ($L_1^{R2-\bullet}$) complexes of $V^{IV}O$ as illustrated in Scheme 2 (vide infra). **1**−**5** are thus oxidizing agents. It is surprising to observe that no

Scheme 2

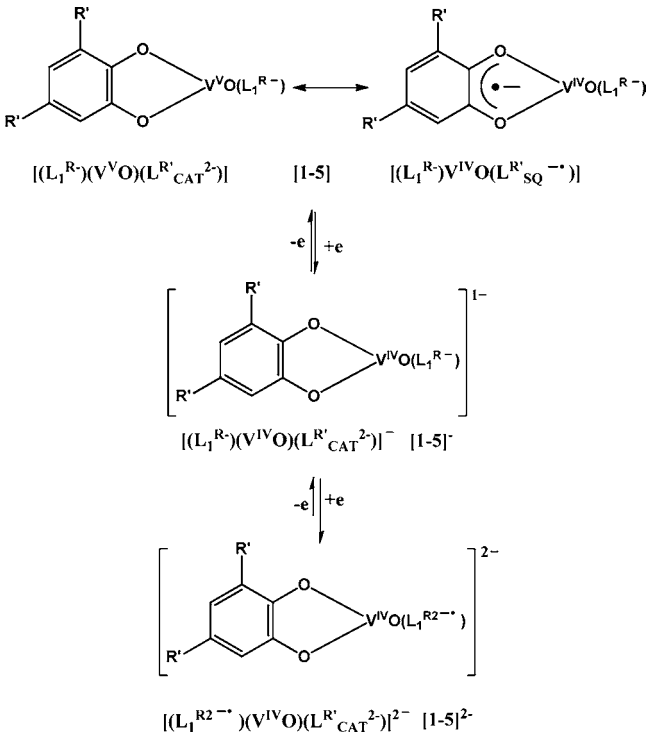

reversible anodic wave of **1**−**5** was detected. The irreversible anodic waves of **1**−**5** at +(0.32−0.45) V (E_p^1) were due to the formations of $[(L^{R'}{}_{Q})(V^{V}O)]$ complexes which are unstable in solutions. The electro-generated paramagnetic reduced $[\mathbf{1}-\mathbf{5}]^-$ complexes were analyzed by UV−vis/NIR, EPR spectra, unrestricted DFT and TD DFT calculations. The dianions $[\mathbf{1}-\mathbf{5}]^{2-}$ were investigated by UV−vis/NIR spectra and DFT calculations.

The EPR spectra of the CH_2Cl_2 frozen glasses of electro-generated $[\mathbf{1}-\mathbf{5}]^-$ were recorded at 78 K. The axial EPR spectrum with the simulations, which correspond to $S = 1/2$ and hyperfine coupling from ^{51}V ($I = 7/2$) of $[\mathbf{2}]^-$ ion, is shown in Figure 5. The EPR spectra of other complexes are illustrated in Supporting Information, Figure S5. EPR parameters are summarized in Table 7 and Supporting Information, Chart S2. The EPR spectra are consistent with the existence of the $[VO]^{2+}$ state in a octahedral coordination sphere[5a,25] with the Type II coordination (Chart 1), that is,

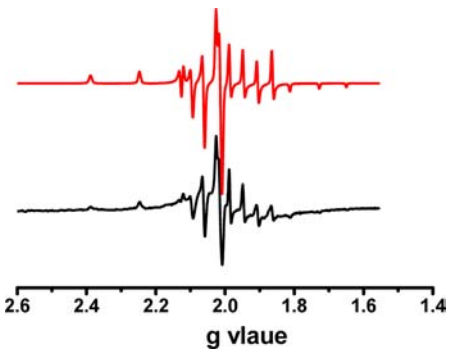

Figure 5. X-band EPR spectra of the frozen CH_2Cl_2 glasses of $[\mathbf{2}]^-$ (black, experimental; red, simulated) at 78 K.

dx.doi.org/10.1021/ic400166z | Inorg. Chem. 2013, 52, 7417−7430

Table 7. X-Band EPR Spectral Parameters of CH_2Cl_2 Frozen Glasses of $[1-5]^-$ at 78 K

comp	$g_{\|}$	$g_{\perp}$	$A_{\|}$ (10^{-4} cm^{-1})	$A_{\perp}$ (10^{-4} cm^{-1})
$[\mathbf{1}]^-$	1.9484	1.9785	162	56
$[\mathbf{2}]^-$	1.9480	1.9787	164	60
$[\mathbf{3}]^-$	1.9480	1.9794	162	57
$[\mathbf{4}]^-$	1.9481	1.9794	163	55
$[\mathbf{5}]^-$	1.9470	1.9775	165	57

diamagnetic catecholato ($L^{R'}{}_{CAT}{}^{2-}$) coordinated to the paramagnetic $[VO]^{2+}$ ion. The g parameters and the hyperfine coupling constants of all the anions are similar. $[\mathbf{1}-\mathbf{5}]^-$ are the first examples of VO^{2+} complexes of catecholates.

In cases of complexes **1**−**5**, the oxidized complexes are unstable. No quinone complexes have been identified. DFT calculations (vide infra) have confirmed the irreversible oxidation is due to the formation of quinone complexes, $[(L_1{}^{R-})(VO^{2+})(L^{R'}{}_Q)]^+$ ($L^{R'}{}_Q$ = substituted *o*-benzoquinone) incorporating the oxidovanadium(IV) ion.

Electronic Structures. BS Density Functional Theory (DFT) Calculations. The bond parameters of the OO-chelates including the aromatic ring of **1**, **2**, **4**, and **5** complexes do not correlate distinctly with the dianionic catecholato or the monoanionic benzosemiquinone state of the ligands. Elucidation of the ground electronic state of the complexes **1**−**5** thus is a subject of theoretical investigation. The electronic structures of the complexes **1**−**5** correlating the experimental bond parameters and the spectral features were investigated by the BS and TD DFT calculations on the less substituted **1** and **3** complexes using B3LYP, B3PW91, and PBE1PBE functionals. The electronic structures of the reduced monoanions and the dianions were elucidated by the unrestricted DFT calculations on $\mathbf{1}^-$, $\mathbf{3}^-$, $\mathbf{1}^{2-}$, and $\mathbf{3}^{2-}$ ions using doublet and triplet spin states, respectively.

Analyses of the frontier molecular orbitals of the gas-phase optimized geometries of **1** and **3** using the singlet spin state at the RB3LYP or RB3PW91 or RPBE1PBE level of the theory have substantiated that the frontier highest occupied molecular orbitals (HOMOs) and lowest unoccupied molecular orbitals (LUMOs) of **1** and **3** are constituted of vanadium d- and catecholato- orbitals as shown in Supporting Information, Figure S6. It is a significant observation to predict the ground electronic state of the complexes **1**−**5**. Analyses of the stabilities of the singlet self-consistent field (SCF) solutions of **1** and **3** using all functionals reported that the lowest Hessian eigenvalues of all these solutions are negative and predicting the CSS solutions of **1** and **3** are unstable with respect to triplet perturbations. For **1**, the eigenvalues are −0.024 with B3LYP and −0.018 with B3PW91 functionals due to HOMO to LUMO excitations. The HOMO of **1** is composed of 76% catechol ligand and 19% vanadium d-orbitals while LUMO is composed of 31% catechol ligand and 60% vanadium d-orbitals. Instability due to the HOMO→LUMO excitation is defined as the closed shell singlet (CSS) → open shell singlet (OSS) perturbation stabilizing the $[VO]^{2+}$ state. The LMCT perturbations of the complexes **1**−**5** were identified at ∼800 nm (see Electronic Spectra section). Similarly, the CSS solutions of **3** are unstable due to OSS perturbation. The lowest Hessian eigenvalues for HOMO to LUMO excitations are −0.027 with B3LYP and −0.022 with B3PW91 functionals.

The instabilities of the CSS solutions suggest two possibilities: (i) the ground electronic state is a singlet diradical that requires an unrestricted BS solution for proper description, or (ii) the triplet state (S = 1) is more stable than the singlet state. The issue is addressed by reoptimizing the unstable CSS solutions using the BS method. The BS solutions with lower energy ensure certain percentage of diradical character in **1** and **3** (**1**: 73% with B3PLYP and 64% with B3PW91 functionals; **3**: 26% with B3PLYP and 72% with B3PW91functionals). The investigation proposes the contribution of the Type III state in **1**−**5** as shown in Chart 2. The percentage of contribution of the diradical Type III state in **1** and **3** of course are different. To define the BS state, the systems are divided into two fragments and the notation BS (1,1) with S_t = 0 refers to a BS state with one unpaired spin-up (with +1/2 spin) electron on the $L^{R'}{}_{SQ}{}^{-\bullet}$ fragment and one unpaired spin-down (with −1/2 spin) electron essentially localized on the $[VO]^{2+}$ core. Bond parameters of the BS (1,1) M_s = 0 solutions of **1** and **3** are similar to those found in the CSS solutions, but the BS (1,1) M_s = 0 solutions are stable under the perturbations considered. Bond parameters of the BS (1,1) M_s = 0 solutions are summarized in Table 3 and Supporting Information, Table S4 and correlate well with those obtained from the single crystal X-ray structure determinations of **1**, **2**, **4**, and **5** complexes.

The features of the triplet state were calculated by optimizing the geometries of **1** and **3** with Type III coordination using triplet states (S = 1) as shown in Chart 1 and same basis sets as for CSS, BS (1,1) M_s = 0 solutions. The calculated bond parameters are listed in the Tables 3 and Supporting Information, Table S4. The triplet solution comparatively has higher energy, and the calculated bond lengths deviate significantly from those obtained from the single crystal X-ray structure determinations and BS (1,1) M_s = 0 solution.

The effect of the redox noninnocent ligand on the electronic structures of **1**−**5** has been justified by performing the similar calculations on a model complex, $[(L_1{}^{R-})(VO)(L_{OO}{}^{2-})]$ (**8**) containing a redox-innocent dianionic (1*R*,2*S*)-cyclohexane-1,2-bis(olate) ligand ($L_{OO}{}^{2-}$). The features of the frontier orbitals of the $[(L_1{}^{R-})(VO)(L_{OO}{}^{2-})]$ (**8**) complex were established by optimizing **8** in the gas phase with a singlet spin state. In contrast to the contribution of the d-orbital to the HOMOs of the singlet **1** and **3**, no contribution of the vanadium d-orbitals to the HOMO of **8** is noted (Supporting Information, Scheme S1). The LUMO of **8** is a pure vanadium d-orbital. The wave function has no instability due to OSS perturbations defining **8** as a pure $[VO]^{3+}$ complex of $L_{OO}{}^{2-}$. The bond parameters of the pure Type I electronic state are summarized in Supporting Information, Scheme S1. In **8**, two C−O lengths of the OO-chelate are longer than those calculated in **1** and **3**. All the V−O lengths are shorter and correlate well with a $[VO]^{3+}$ coordination sphere.[5]

$[(L_1{}^{R-})(VO^{3+})(L^{R'}{}_{CAT}{}^{2-})]$ (Type I) versus $[(L_1{}^{R-})(VO^{2+})(L^{R'}{}_{SQ}{}^{-\bullet})]$ (Type III) States. Formal charges of the ligands and the oxidovanadium ion of the complexes **1**−**5** are balanced by the closed shell Type I coordination. However, the experimental bond parameters of **1** (Table 3), **2**, **4**, and **5** (Supporting Information, Tables S1−S3) deviate significantly from a Type I coordination. DFT calculations have authenticated that the CSS solutions of **1** and **3** are unstable with respect to OSS perturbations. BS (1,1) M_s = 0 solutions are stable contributing respectively 72% and 25% diradical state (Type IV) to **1** and **3**. It instigates the resonance contributions of Type I and III electronic states (Chart 2) to complexes **1**−**5**. The BS (1,1) M_s = 0 solutions of **1** are stabilized by 8.79 and

dx.doi.org/10.1021/ic400166z | Inorg. Chem. 2013, 52, 7417−7430

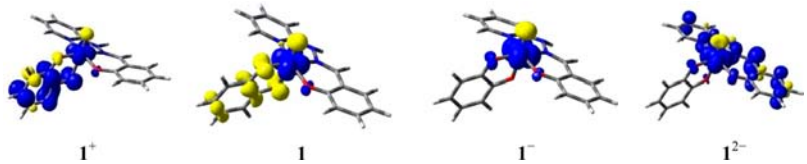

Figure 6. Spin density plots of $\mathbf{1}^{+}$, **1**, $\mathbf{1}^{-}$, and $\mathbf{1}^{2-}$ (blue, α spin; yellow, β spin) and values from Mulliken spin population analyses (spin density, $\mathbf{1}^{+}$: V 0.32, O1 −0.05, O21 0.25, O22 −0.04, O16 0.01, C21 0.03, C22 0.26, C23 −0.16, C24 0.31, C25 −0.07, C26 0.14; **1**: V 0.72, O1 −0.10, O21 −0.16, O22 −0.16, O16 0.01, N1 −0.01, C21 −0.07, C22 −0.09, C24 −0.08, C25 −0.06, C26 −0.01; $\mathbf{1}^{-}$: V 1.07, O1 −0.14, O16 0.02, O22 0.03; $\mathbf{1}^{2-}$: V 1.09, O1 −0.09, O16 0.05, O22 0.03, N1 0.09, N7 −0.02, N8 0.11, C23 0.02, C2 0.02, C3 0.01, C4 0.14, C5 −0.04, C6 0.06, C9 0.30, C10 −0.08, C11 0.16, C12 −0.07, C13 0.15, C15 0.07).

5.20 kJ/mol compared to the CSS solutions respectively with B3LYP and B3PW91 functionals. Similarly, at the B3LYP level of the theory, the BS (1,1) M_s = 0 solution of **3** is stabilized by 6.83 kJ/mol. Compared to the BS (1,1) M_s = 0 solution, the BS (1,1) M_s = 1 solution is destabilized by 13.87 kJ/mol. The gas phase optimized geometry of **3** is shown in Supporting Information, Figure S7. The calculated bond parameters of the BS (1,1) M_s = 0 and BS (1,1) M_s = 1 solutions of **1** and **3** are listed in Table 3 and Supporting Information, Table S4 for comparison. The calculated bond parameters of the BS (1,1) M_s = 1 solutions particularly of the coordination sphere and the OO-chelate are quite different. Mulliken spin population of the BS (1,1) M_s = 0 solutions of **1** and **3** are depicted in Figure 6 and Supporting Information, Figure S8. Calculated atomic spins are listed under the caption of Figure 6 and Supporting Information, Figure S8. The calculations affirm the contribution of the $[VO]^{2+}$ state in complexes **1**−**5** as recognized by the localized alpha spin on the vanadium center of **1** and **3**.

The calculated V−O lengths of the OO-chelate are dissimilar. One of the V−O lengths is comparatively longer due to the trans influence of the V=O bond[5] and reproduces well the experimental trend. Two C−O lengths, 1.295 and 1.330 Å (average lengths, 1.312 Å) in **1** and 1.293 and 1.328 Å (average lengths, 1.310 Å) in **3** are not consistent with the existence of the pure dianionic catecholato (average C−O lengths, 1.35 ± 1 Å) or the monoanionic benzosemiquinone (average C−O lengths, 1.30 ± 1 Å) ligand in the complexes **1**−**5**. The experimental average C−O lengths of the OO-chelate are 1.326(2) for **1**, 1.324(2) for **2**, 1.336(3) for **4**, and 1.329(3) Å for **5**. The calculated quinoidal distortion of the aromatic phenyl ring with the adjacent long−short−long−short C−C bonds (Table 3 and Supporting Information, Table S4) is similar to those observed in the experimental lengths. These length trends correlate satisfactorily with the contribution of Type I and Type III tautomers in complexes **1**−**5** as depicted in Chart 2.

$[(L_1^{R-})(VO^{2+})(L^{R'}{}_{CAT}{}^{2-})]^{-}$ (Type II Coordination). The spin density distribution of the paramagnetic $[\mathbf{1}-\mathbf{5}]^{-}$ ions were analyzed by the unrestricted DFT calculations on $\mathbf{1}^{-}$ and $\mathbf{3}^{-}$ ions. The spin density plots obtained from the Mulliken spin population analyses are shown in Figure 6 and Supporting Information, Figure S8 which confirm the existence of the oxidovanadium(IV) ion in $[\mathbf{1}-\mathbf{5}]^{-}$ ions. In $\mathbf{1}^{-}$ and $\mathbf{3}^{-}$, the spin density is primarily localized on the oxidovanadium ion corroborating the EPR spectra of the frozen glasses of the reduced ions. $[\mathbf{1}-\mathbf{5}]^{-}$ ions are thus defined as the catecholato complexes of the $[VO]^{2+}$ ion incorporating the coordination Type II which is not reported in the literature so far. The C−O lengths are elongated to average lengths of 1.328 from 1.312 Å in case of **1** and 1.327 from 1.310 Å in case of **3**. No quinoidal distortion of the phenyl ring is noted. The V(1)−O(39) length increases by 0.1 Å. It predicts the higher affinity of the benzosemiquinone ligand ($L^{H}{}_{SQ}{}^{-\bullet}$) toward the paramagnetic oxidovanadium(IV) ion as observed with the paramagnetic *o*-iminobenzosemiquinone anion radical complexes.[5] The bond parameters of the hydrazone ligand remains unchanged during the transformations of **1** and **3** to $\mathbf{1}^{-}$ and $\mathbf{3}^{-}$ ions.

$[(L_1^{R2-\bullet})(VO^{2+})(L^{R'}{}_{CAT}{}^{2-})]^{2-}$ (Type II Coordination). The origin of the quasi-reversible or irreversible reduction waves ($E_p{}^3$, Table 6) of complexes **1**−**5** at −0.80 to −1.32 V versus Fc^{+}/Fc couple is a subject of investigation. The dianions are identified by spectro-electrochemical measurements. CSS solutions of $\mathbf{1}^{2-}$ and $\mathbf{3}^{2-}$ are unstable. However, BS (1,1) M_s = 1 solutions are more stable (∼ 24 kJ/mol) than BS (1,1) M_s = 0 solutions. The spin density plots of the triplet solutions of $\mathbf{1}^{2-}$ and $\mathbf{3}^{2-}$ ions are illustrated in Figure 6 and Supporting Information, Figure S8. It is surprising to note that the tridentate hydrazone ligand is reduced to radical dianion in $\mathbf{1}^{2-}$ and $\mathbf{3}^{2-}$ ions and coordinated to the $[VO]^{2+}$ ion. It predicts that $L_1{}^{R-}$ hydrazone ligand is also redox-active. The calculated bond parameters of the $\mathbf{1}^{2-}$ and $\mathbf{3}^{2-}$ ions are summarized in Table 3 and Supporting Information, Table S4. In the dianions, the average −CH=N- (hydrazone) length is 1.330 Å, and the dianions are defined as $[(L_1{}^{R2-\bullet})(VO^{2+})(L^{R'}{}_{CAT}{}^{2-})]^{2-}$.

$[(L_1^{R-})(VO^{3+})(L^{R'}{}_{SQ}{}^{-\bullet})]^{+}$ (Type IV Coordination). The one-electron anodic waves ($E_p{}^1$, Table 6) of the complexes **1**−**5** are irreversible. The electronic state of the oxidized analogues was elucidated by the unrestricted DFT calculations on $\mathbf{1}^{+}$ and $\mathbf{3}^{+}$ ions. The calculated spin density distribution obtained from the Mulliken spin population analyses are shown in Figure 6 and Supporting Information, Figure S8. Bond parameters are listed in Table 3 and Supporting Information, Table S4. Spin density distribution of $\mathbf{1}^{+}$ and $\mathbf{3}^{+}$ ions predicts the contribution of both the valence tautomers, that is, benzoquinone coordinated to the $[VO]^{2+}$ ion or the *o*-benzosemiquinone coordinated to the $[VO]^{3+}$ ion in $[\mathbf{1}-\mathbf{5}]^{+}$ ions. The calculated $[VO]^{2+}$ state in $\mathbf{1}^{+}$ is 32% while it is 96% in the $\mathbf{3}^{+}$ ion. The electronic state of the cations is defined by the resonance structures of Type V and Type IV electronic states. This observation supports the contribution of Type I and Type III coordinations to the ground electronic state of complexes **1**−**5**. This observation completely contrasts the redox features of the corresponding *o*-aminophenol complexes of the oxidovanadium ion, which undergo two successive reversible oxidations due to formation of *o*-iminobenzoquinone complexes of $[VO]^{2+}$ and $[VO]^{3+}$ ions.[5a]

Electronic Spectra. The UV−vis/NIR absorption spectra of **1**−**5** in CH_2Cl_2 are shown in Figure 1. All the complexes absorb characteristically at 550 and 800 nm. However, these lower energy absorption bands disappear upon reduction in all cases as observed in spectro-electrochemical and coulometric

dx.doi.org/10.1021/ic400166z | Inorg. Chem. 2013, 52, 7417−7430

measurements. The changes of spectral features due to the transformations of $[\mathbf{1}-\mathbf{5}]\rightarrow[\mathbf{1}-\mathbf{5}]^{-}$ and $[\mathbf{1}-\mathbf{5}]^{2-}$ anions in CH_2Cl_2 are shown in Figure 7 and Supporting Information,

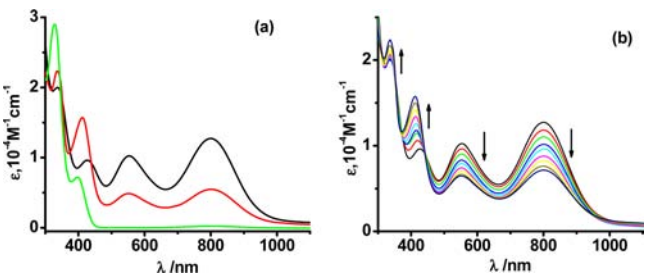

Figure 7. Electronic absorption spectra of (a) electrogenerated $\mathbf{2}^{2-}$ (green), $\mathbf{2}^{-}$ (red) ions and **2** (black) and (b) spectroelectrochemistry of $[\mathbf{2}\rightarrow\mathbf{2}^{-}]$ in CH_2Cl_2 at 298 K.

Figure S9, and the spectral data are summarized in Table 2. To explain the spectral features TD DFT calculations were carried out on **1**, **3**, $\mathbf{1}^{-}$, $\mathbf{3}^{-}$, and $\mathbf{1}^{2-}$ ions. Analyses of the excitation energies conclude that the lower energy absorption bands at >500 nm in **1**−**5** are due to the charge transfer from the $L^{R'}{}_{CAT}{}^{2-}$ ligand to [VO] core. This charge transfer is defined as CSS-OSS perturbations charge transfer. The charge transfer is disallowed after the first reduction due to formation of the $V^{IV}O$ state, and the lower energy bands disappear in $[\mathbf{1}-\mathbf{5}]^{-}$ anions.

Analyses of the TD DFT calculations on $\mathbf{1}^{-}$ and $\mathbf{3}^{-}$ ions have substantiated that $[\mathbf{1}-\mathbf{5}]^{-}$ ions absorb weakly at >500 nm due to the charge transfer of $L^{R'}{}_{CAT}{}^{2-}$ to $L_1{}^{R-}$ ligand (LLCT) and mixed metal ligand to ligand charge transfer (MMLLCT). Absorption of the dianions $[\mathbf{1}-\mathbf{5}]^{2-}$ are due to intraligand charge transfer (ILCT) within $L_1{}^{R2-\bullet}$ ligand and LLCT and the charge transfer from the $L_1{}^{R2-\bullet}$ to the [VO] core as listed in the Supporting Information, Table S5. The calculated spectra of **1**, $\mathbf{1}^{-}$, and $\mathbf{1}^{2-}$ ions are illustrated in Supporting Information, Figure S10 which authenticates the disappearance of the absorption bands in the region of 1000−400 nm upon stepwise reductions as observed in Figures 7 and Supporting Information, Figure S9.

The solid state absorption spectra (Kubelka−Munk plot)[26] of **1**−**5** were recorded by the diffuse reflection method. It is significant to observe that the lower energy absorption maxima of **1**−**5** are red-shifted in solids. The absorption maxima (λ_{max}) are as follows: **1**, 960 (solid) and 802 (CH_2Cl_2); **2**, 965 (solid) and 801 (CH_2Cl_2); **3**, 995 (solid) and 811 (CH_2Cl_2); **4**, 875 (solid) and 786 (CH_2Cl_2); **5**, 936 (solid) and 794 (CH_2Cl_2) nm. The origin of these bands is the CSS-OSS perturbation, that is, LMCT authenticated by the TDDFT calculations. The red shift of the absorption maxima in solids indicates the stabilization of the HOMO based on the catecholato ligand in solution. The LMCT transition results in the conversion of the catecholato to the benzosemiquinone state promoting $[(L_1{}^{R-})(VO^{3+})(L^{R'}{}_{CAT}{}^{2-})]$ (Type I) ↔ $[(L_1{}^{R-})(VO^{2+})(L^{R'}{}_{SQ}{}^{-\bullet})]$ (Type III) equilibrium which is expectedly temperature dependent. The solid state spectra of **1** at 273, 298, and 320 K are recorded, and the spectra are illustrated in Figure 8. It is noted that with the change of temperature, λ_{max} does not change significantly; however, the intensity of the transition changes. At 273 K, the intensity of transition is higher, while it decreases with rise of temperature. The result implies that the

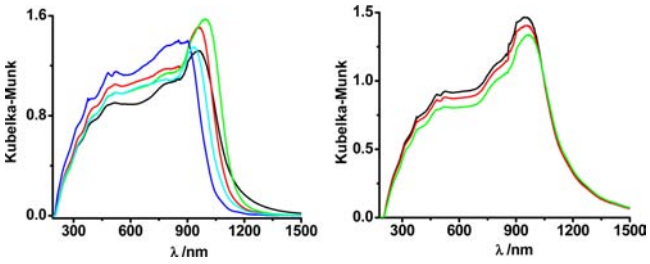

Figure 8. (a) Solid state UV−vis/NIR absorption spectra (Kubelka−Munk plot) of **1** (black), **2** (red), **3** (green), **4** (blue), and **5** (olive) at 298 K and (b) temperature dependent spectra of **1** at 273 K (black), 298 K (red), and 320 K (green).

contributions of the Type I state increase at lower temperature, while the contributions of Type III state increase with increase in temperature. Similar features of the temperature dependent solid state spectra due to valence tautomerism have been reported by Pierpont et al.,[27] particularly on $[Mn^{IV}(2,2\text{-bpy})(3,6\text{-DBCat})_2]$ ↔ $[Mn^{III}(2,2\text{-bpy})(3,6\text{-DBSQ})(3,6\text{-DBCat})]$ equilibrium.[28]

DISCUSSION

Elucidation of the electronic structures of the oxidovanadium catechol complexes is a subject of investigation.[4b,c,24] In this work, a new family of oxidovanadium complexes of type $[(L_1{}^{R})(VO)(L^{R'})]$ (R = H, R′ = H, **1**; R = H, R′ = -CMe_3, **2**; R = H, R′ = Me, **3**; R = -CMe_3, R′ = H, **4**; R = -CMe_3, R′ = -CMe_3, **5**) incorporating substituted catechols ($L^{R'}H_2$) and 2,4-di-R-6-{(2-(pyridin-2-yl)hydrazono)methyl}phenol ($L_1{}^{R}H$) were isolated. The single crystal X-ray structural bond parameters of **1**−**5** (Table 3 and Supporting Information, Tables S1−S3) do not correlate with the $[(L_1{}^{R-})(VO^{3+})(L^{R'}{}_{CAT}{}^{2-})]$ descriptions. The MOS of the catechols have been calculated (Table 4).[21] The MOS of the catechols vary from −1.43 to −1.60. Ignoring the contribution of $L^{R'}{}_{Q}$ states, the fractional MOSs are analyzed by the presence of dianionic $L^{R'}{}_{CAT}{}^{2-}$ and monoanionic $L^{R'}{}_{SQ}{}^{-\bullet}$ states in **1**−**5** (Table 4).[22] The average contributions of them are around 50% each. These results predict that the catechol ligands are redox noninnocent toward the oxidovanadium(IV) ion and furnish redox isomers of oxidovanadium(IV) coupled to $L^{R'}{}_{SQ}{}^{-\bullet}$.

The redox noninnocence of the catechol ligands toward the oxidovanadium ion was investigated by the CP MAS and solution ^{51}V NMR spectra. ^{51}V NMR spectral features are important to analyze the electronic state of the oxidovanadium ion. The method was primarily introduced by Pecoraro et al.[4b,c] and Crans et al.[24] The ^{51}V NMR spectra of the solid and solutions of **1**−**5** are illustrated in Figure 3 and Supporting Information, Figure S3. Chemical shifts of **1**−**5** span the positive region (Table 5). The chemical shifts of **1**−**5** are compared with the chemical shifts of *o*-iminobenzosemiquinone radical ($L^{H}{}_{IS}{}^{-\bullet}$) complexes of the oxidovanadium(IV), $[(L_1{}^{H-})(VO^{2+})(L^{H}{}_{IS}{}^{-\bullet})]$ (**6**) and $[(L_1{}^{t\text{-}Bu-})(VO^{2+})(L^{H}{}_{IS}{}^{-\bullet})]$ (**7**).[5a] The isotropic chemical shifts of **1**−**7** complexes are comparable. In DMSO-d_6, ^{51}V nuclei are more deshielded (^{51}V CP MAS: −19.8 to +248.6 ppm; DMSO-d_6: +173.9 to +414.55 ppm). The chemical shifts of **1**−**7** differ significantly from the common $[VO]^{3+}$ complexes.[29] However, this trend of chemical shifts are common with the strongly coupled binuclear

dx.doi.org/10.1021/ic400166z | Inorg. Chem. 2013, 52, 7417−7430

oxidovanadium(IV) complexes. It is reported that the ^{51}V nuclei are deshielded in the binuclear coupled systems even at +1237 ppm.[29] The deshielding in **1**−**7** can be correlated with the existence of the oxidovanadium(IV) ion coupled to $L^{R'}{}_{SQ}{}^{-\bullet}$ or $L^{H}{}_{IS}{}^{-\bullet}$. The ^{13}C NMR spectra also support the oxidation of the catechols to *o*-semiquinone radicals. In **1**−**7**, the C−O carbon atoms are deshielded. The similar observations are documented in the conversions of the catechols to quinones.[23]

The X-ray structural bond parameters and the ^{51}V NMR spectral data have been analyzed by the DFT calculations on **1** and **3**. One of the significant observations is that the CSS solutions of **1** and **3** are unstable due to the OSS perturbations. The BS (1,1) S_t = 0 states are stable and produce the bond parameter closely. It is consistent with the existence of the diradicals, that is, oxidovanadium(IV) ion coupled to $L^{R'}{}_{SQ}{}^{-\bullet}$ in **1**−**5**. The contributions of the diradical state (Type III electronic state) to the ground electronic state of complexes **1**−**5** thus have been predicted. However, the percentage of the contributions of the Type III state in **1** and **3** are different. Both the bond parameters of the redox noninnocent catechols and the chemical shifts are analyzable by the existence of the diradical Type III state in **1**−**5**. The calculated ^{51}V NMR parameters on the single crystal X-ray and optimized geometries of **1** are similar to those obtained from the CP MAS ^{51}V nuclei resonances (Table 5).

The strong NIR absorption bands of **1**−**5** (Table 2) in solution and solid are the manifestations of the instabilities of the CSS-states due to OSS perturbation. The transition intensity of the solid depends on temperature. This charge transfer has been defined as CSS-OSS metal to ligand charge transfer elucidated by the TD DFT calculations. It is expected that the lower the energy of transition, the higher will be the contribution of the diradical Type III state. Thus, redox noninnocence of the catechols toward the oxidovanadium(V) ion can be correlated with the NIR absorption bands of the complexes. Similar features have been reported by Pecoraro et al.[4b,c]

Complexes **1**−**5** display two cathodic waves. The one-electron reduced paramagnetic analogues, $[(L_1{}^{R-})(VO^{2+})(L^{R'}{}_{CAT}{}^{2-})]^{-}$, $[\mathbf{1}-\mathbf{5}]^{-}$, were investigated by spectro-electrochemical measurements and EPR spectra. The second reduction is not metal centered, rather it generates hydrazone anion radical complexes $[(L_1{}^{R2-\bullet})(VO^{2+})(L^{R'}{}_{CAT}{}^{2-})]^{2-}$ of oxidovanadium(IV), with Type II (S = 1) electronic state. The anodic waves of complexes **1**−**5** are irreversible inferring that $L^{R'}{}_{Q}$ complexes of Types V and VI (Chart 1) are unstable.

On the contrary, the similar *o*-aminophenol analogues[5a] were defined as *o*-iminobenzosemiquinone ($L^{R'}{}_{IS}{}^{-\bullet}$) complexes of oxidovanadium(IV) ion, $[(L_1{}^{R-})(VO^{2+})(L^{R'}{}_{IS}{}^{-\bullet})]$ as depicted in Chart 2. The MOSs of the coordinated *o*-aminophenols using X-ray structural and DFT calculated parameters are calculated and compared with those of **1**−**5**. The data are presented in Supporting Information, Table S6. The calculations show that the diradicals Type III state incorporating *o*-iminobenzosemiquinone anion radical ($L^{R'}{}_{IS}{}^{-\bullet}$) coupled to oxidovanadium(IV) is dominant here. The redox series of these two families are surprisingly contrasting. $L^{R'}{}_{IS}{}^{-\bullet}$ complexes of oxidovanadium(IV) ion undergo two successive reversible oxidations to *o*-iminobenzoquinone ($L^{R'}{}_{IQ}$) complexes of VO^{2+} and VO^{3+} as illustrated in Scheme 3, while the catechol complexes, $[(L_1{}^{R})(VO)(L^{R'})]$ undergo two successive reductions (Scheme 2).

Scheme 3

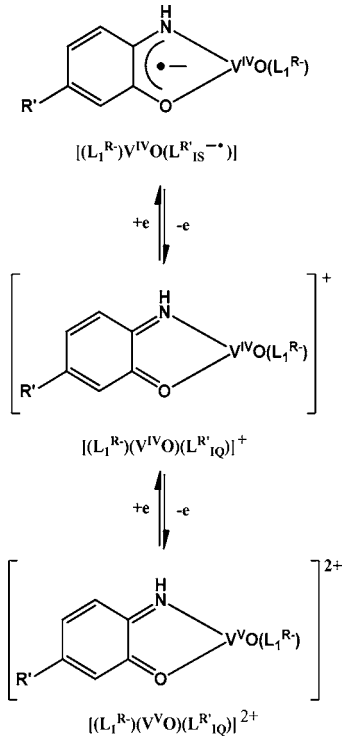

CONCLUSION

In conclusion, X-ray bond parameters, MOS, CP MAS and DMSO-d_6 ^{51}V NMR spectra, NIR absorption bands, and BS DFT calculations authenticated that the catechol ligands in **1**−**5** are redox noninnocent. The ground electronic structures of **1**−**5** are analyzed by the resonance structures of the catecholates coordinated to oxidovanadium(V) ion (Type I electronic state) and *o*-benzosemiquinone radical coordinated to oxidovanadium(IV) ion (Type III electronic state) as illustrated in Scheme 2. The complexes are oxidizing in nature while the corresponding *o*-aminophenol analogues are defined as $[(L_1{}^{R-})(VO^{2+})(L^{R'}{}_{IS}{}^{-\bullet})]$ incorporating a Type III electronic state and are reducing in nature ($L^{R'}{}_{IS}{}^{-\bullet}$ = *o*-iminobenzosemiquinone). The redox series of **1**−**5** and $[(L_1{}^{R-})(VO^{2+})(L^{R'}{}_{IS}{}^{-\bullet})]$ complexes are summarized in Schemes 2 and 3. It is an unprecedented example of tuning of redox features of the oxidovanadium(IV/V) ions upon coordination of redox noninnocent catechol and *o*-aminophenol ligands.

ASSOCIATED CONTENT

Supporting Information

X-ray crystallographic CIF files for the **1**, **2**, **4**, and **5** complexes; experimental bond parameters of **2**, **4**, and **5** (Table S1−S3); comparative bond lengths of the catecholato fragments (Chart S1); molecular geometries of **4** and **5** (Figure S1); intermolecular H-bonding interactions in **2** (Figure S2); ^{51}V CP MAS spectra and ^{51}V NMR in DMSO-d_6 of complexes **1**−**7** (Figure S3); cyclic voltammograms of **1**, **3**, **4**, **5** (Figure S4); X-

dx.doi.org/10.1021/ic400166z | Inorg. Chem. 2013, 52, 7417−7430

band EPR spectra of 1^-, 3^-, 4^-, and 5^- (Figure S5) and experimental EPR parameters (Chart S2); frontier molecular orbitals of **1** and **3** (Figure S6); frontier orbitals and selected calculated bond lengths of **8** (Scheme S1); optimized geometry of **3** (Figure S7); selected calculated bond parameters of **3**, 3^+, 3^- and 3^{2-} (Table S4); spin density plot of 3^+, **3**, 3^-, and 3^{2-} (Figure S8); electronic absorption spectra of **1**−**5** and electrogenerated $[1-5]^-$ and $[1-5]^{2-}$ ions; spectro-electrochemical measurements (Figure S9); electronic absorption spectra of **1**, 1^- and 1^{2-} obtained from TD DFT calculations (Figure S10); excitation energies, oscillator strengths, transition types, and dominant contributions of UV−vis/NIR absorption bands of **1**, **3**, 1^-, 3^-, and 1^{2-} obtained from TD DFT calculations (Table S5); MOS Analyses of **6** and **7** (Table S6); and the optimized coordinates of **1** ($S = 0$), **1** ($S = 1$), **3** ($S = 0$), **3** ($S = 1$), 1^+ ($S = 1/2$), 1^- ($S = 1/2$), 1^{2-} ($S = 1$), 3^+ ($S = 1/2$), 3^- ($S = 1/2$), 3^{2-} ($S = 0$), and **8** ($S = 0$) (Tables S7−S21). This material is available free of charge via the Internet at http://pubs.acs.org.

AUTHOR INFORMATION

Corresponding Author

*E-mail: ghosh@pghosh.in. Phone: +91-33-2428-7347. Fax: +91-33-2477-3597.

Author Contributions

The manuscript was written through contributions of all authors. All authors have given approval to the final version of the manuscript.

Notes

The authors declare no competing financial interest.

ACKNOWLEDGMENTS

Financial support received from DST (SR/S1/IC/0026/2012) and CSIR (3231/NS-EMRII) New Delhi, India, is gratefully acknowledged. S.K. and S.M. are thankful to CSIR, New Delhi, India, for fellowships. We are gratefully to Dr. P. R. Rajamohanan and Central NMR Facility, National Chemical Laboratory, Pune, India. for recording the ^{51}V NMR spectra.

REFERENCES

(1) Representative references are as follows: (a) Pessoa, J. C.; Tomaz, I. *Curr. Med. Chem.* **2010**, *17*, 3701−3738. (b) Aureliano, M.; Crans, D. C. *J. Inorg. Biochem.* **2009**, *103*, 536−546. (c) Li, M.; Ding, W.; Baruah, B.; Crans, D. C.; Wang, R. *J. Inorg. Biochem.* **2008**, *102*, 1846−1853. (d) Crans, D. C.; Baruah, B.; Gaidamauskas, E.; Lemons, B. G.; Lorenz, B. B.; Johnson, M. D. *J. Inorg. Biochem.* **2008**, *102*, 1334−1347. (e) Schneider, C. J.; Penner-Hahn, J. E.; Pecoraro, V. L. *J. Am. Chem. Soc.* **2008**, *130*, 2712−2713. (f) Rehder, D. *Bioinorganic Vanadium Chemistry*; John Wiley & Sons, Ltd.: New York, 2008; (g) Rehder, D. *Org. Biomol. Chem.* **2008**, *6*, 957−964. (h) Drouza, C.; Keramidas, A. D. *Inorg. Chem.* **2008**, *47*, 7211−7224. (i) Schneider, C. J.; Pecoraro, V. L. *Vanadium: The Versatile Metal*; ACS Syposium Series 974; American Chemical Society: Washington, DC, 2007; 148−162; (j) Schneider, C. J.; Zampella, G.; Greco, C.; Pecoraro, V. L.; Gioia, L. D. *Eur. J. Inorg. Chem.* **2007**, *4*, 515−523. (k) Zampella, G.; Fantucci, P.; Pecoraro, V. L.; Gioia, L. D. *Inorg. Chem.* **2006**, *45*, 7133−7143. (l) Zampella, G.; Fantucci, P.; Pecoraro, V. L.; Gioia, L. D. *J. Am. Chem. Soc.* **2005**, *127*, 953−960. (m) Kravitz, J. Y.; Pecoraro, V. L. *Pure Appl. Chem.* **2005**, *77*, 1595−1605. (n) Crans, D. C.; Smee, J. J.; Gaidamauskas, E.; Yang, L. *Chem. Rev.* **2004**, *104*, 849−902. (o) Maurya, M. R. *Coord. Chem. Rev.* **2003**, *237*, 163−181. (p) Michibata, H.; Yamaguchi, N.; Uyama, T.; Ueki, T. *Coord. Chem. Rev.* **2003**, *237*, 41−51. (q) Smith, T. S., II; LoBrutto, R.; Pecoraro, V. L. *Coord. Chem. Rev.* **2002**, *228*, 1−18. (r) Drouza, C.; Tolis, V.; Gramlich, V.; Raptopoulou, C.; Terzis, A.; Sigalas, M. P.; Kabanos, T. A.; Keramidas, A. D. *Chem. Commun.* **2002**, 2786−2787. (s) Thompson, K. H.; Orvig, C. *Coord. Chem. Rev.* **2001**, *219*−*221*, 1033−1053. (t) Rehder, D. *Coord. Chem. Rev.* **1999**, *182*, 297−322. (u) Taylor, S. W.; Kammerer, B.; Bayer, E. *Chem. Rev.* **1997**, *97*, 333−346. (v) Slebodnick, C.; Hamstra, B. J.; Pecoraro, V. L. *Modelling the Biological Chemistry of Vanadium: Structural and Reactivity Studies Elucidating Biological Function: Structure and Bonding*; Sadler, P., Ed.; Springer: Berlin, Germany, 1997, *89*, 57; (w) Butler, A.; Carrano, C. *J. Coord. Chem. Rev.* **1991**, *109*, 61−105.

(2) (a) Frey, P. A.; Hegeman, A. D.; Reed, G. H. *Chem. Rev.* **2006**, *106*, 3302−3316. (b) Himo, F. *Biochim. Biophys. Acta* **2005**, *1707*, 24−33. (c) Layer, G.; Heinz, D. W.; Jahn, D.; Schubert, W. D. *Curr. Opin. Chem. Biol.* **2004**, *8*, 468−476. (d) Marsh, E. N. G.; Patwardhan, A.; Huhta, M. S. *Bioorg. Chem.* **2004**, *32*, 326−340. (e) Banerjee, R. *Chem. Rev.* **2003**, *103*, 2081−2082. (f) Frey, P. *Annu. Rev. Biochem.* **2001**, *70*, 121−148. (g) Stubbe, J.; van der Donk, W. A. *Chem. Rev.* **1998**, *98*, 705−762.

(3) Representative references are as follows: (a) Pierpont, C. G. *Inorg. Chem.* **2011**, *50*, 9766−9772. (b) Das, D.; Sarkar, B.; Mondal, T. K.; Mobin, S. M.; Fiedler, J.; Kaim, W.; Lahiri, G. K. *Inorg. Chem.* **2011**, *50*, 7090−7098. (c) Verma, P.; Weir, J.; Mirica, L.; Daniel, T.; Stack, P. *Inorg. Chem.* **2011**, *50*, 9816−9825. (d) Das, A. K.; Sarkar, B.; Fiedler, J.; Zális, S.; Hartenbach, I.; Strobel, S.; Lahiri, G. K.; Kaim, W. *J. Am. Chem. Soc.* **2009**, *131*, 8895−8902. (e) Poddel'sky, A. I.; Cherkasov, V. K.; Abakumov, G. A. *Coord. Chem. Rev.* **2009**, *253*, 291−334. (f) Das, D.; Das, A. K.; Sarkar, B.; Mondal, T. K.; Mobin, S. M.; Fiedler, J.; Záliš, S.; Urbanos, F. A.; Jiménez-Aparicio, R.; Kaim, W.; Lahiri, G. K. *Inorg. Chem.* **2009**, *48*, 11853−11864. (g) Mukherjee, C.; Weyhermüller, T.; Bothe, E.; Chaudhuri, P. *Inorg. Chem.* **2008**, *47*, 2740−2746. (h) Kokatam, S. -L.; Chaudhuri, P.; Weyhermüller, T.; Wieghardt, K. *Dalton Trans.* **2007**, 373−378. (i) Mukherjee, C.; Weyhermüller, T.; Bothe, E.; Rentschler, E.; Chaudhuri, P. *Inorg. Chem.* **2007**, *46*, 9895−9905. (j) Mukherjee, S.; Weyhermüller, T.; Bill, E.; Wieghardt, K.; Chaudhuri, P. *Inorg. Chem.* **2005**, *44*, 7099−7108. (k) Min, K. S.; Weyhermüller, T.; Wieghardt, K. *Dalton Trans.* **2004**, 178−186. (l) Min, K. S.; Weyhermüller, T.; Wieghardt, K. *Dalton Trans.* **2003**, 1126−1132. (m) Chun, H.; Verani, C. N.; Chaudhuri, P.; Bothe, E.; Bill, E.; Weyhermüller, T.; Wieghardt, K. *Inorg. Chem.* **2001**, *40*, 4157−4166. (n) Pierpont, C. G. *Coord. Chem. Rev.* **2001**, *219*−*221*, 415−433. (o) Pierpont, C. G.; Attia, A. S. *Collect. Czech. Chem. Commun.* **2001**, *66*, 33−51. (p) Chaudhuri, P.; Verani, C. N.; Bill, E.; Bothe, E.; Weyhermüller, T.; Wieghardt, K. *J. Am. Chem. Soc.* **2001**, *123*, 2213−2223. (q) Pierpont, C. G.; Buchanan, R. M. *Coord. Chem. Rev.* **1981**, *38*, 45−87.

(4) (a) Baruah, B.; Das, S.; Chakravorty, A. *Inorg. Chem.* **2002**, *41*, 4502−4508. (b) Cornman, C. R.; Kampf, J.; Pecoraro, V. L. *Inorg. Chem.* **1992**, *31*, 1981−1983; and *Inorg. Chem.* **1992**, *31*, 1983−1985. (c) Cornman, C. R.; Colpas, G. J.; Hoeschele, J. D.; Kampf, J.; Pecoraro, V. L. *J. Am. Chem. Soc.* **1992**, *114*, 9925−9933. (d) Cooper, S. R.; Koh, Y. B.; Raymond, K. N. *J. Am. Chem. Soc.* **1982**, *104*, 5092−5102.

(5) (a) Kundu, S.; Maity, S.; Maity, A. N.; Ke, S. -C.; Ghosh, P. *Dalton Trans.* **2013**, *42*, 4586−4601. (b) Roy, A. S.; Saha, P.; Adhikary, N. D.; Ghosh, P. *Inorg. Chem.* **2011**, *50*, 2488−2500.

(6) Rowe, R. A.; Jones, M. M. *Inorg. Synth.* **1957**, *5*, 113−115.

(7) (a) Patil, S. A.; Weng, C.-M.; Huang, Po-C.; Hong, F.-E. *Tetrahedron.* **2009**, *65*, 2889−2897. (b) Cameron, P. A.; Gibson, V. C.; Redshaw, C.; Segal, J. A.; White, A. J. P.; Williams, D. J. *Dalton Trans.* **2002**, 415−422. (c) Kannappan, R.; Tanase, S.; Mutikainen, I.; Turpeinen, U.; Reedjick, J. *Inorg. Chim. Acta* **2005**, *358*, 383−388.

(8) (a) Sheldrick, G. M. *ShelXS97*; Universität Göttingen: Göttingen, Germany, 1997. (b) Sheldrick, G. M. *ShelXL97*; Universität Göttingen: Göttingen, Germany, 1997.

(9) Frisch, M. J.; Trucks, G. W.; Schlegel, H. B.; Scuseria, G. E.; Robb, M. A.; Cheeseman, J. R.; Montgomery, Jr., J. A.; Vreven, T.; Kudin, K. N.; Burant, J. C.; Millam, J. M.; Iyengar, S. S.; Tomasi, J.; Barone, V.; Mennucci, B.; Cossi, M.; Scalmani, G.; Rega, N.; Petersson, G. A.; Nakatsuji, H.; Hada, M.; Ehara, M.; Toyota, K.;

Fukuda, R.; Hasegawa, J.; Ishida, M.; Nakajima, T.; Honda, Y.; Kitao, O.; Nakai, H.; Klene, M.; Li, X.; Knox, J. E.; Hratchian, H. P.; Cross, J. B.; Bakken, V.; Adamo, C.; Jaramillo, J.; Gomperts, R.; Stratmann, R. E.; Yazyev, O.; Austin, A. J.; Cammi, R.; Pomelli, C.; Ochterski, J. W.; Ayala, P. Y.; Morokuma, K.; Voth, G. A.; Salvador, P.; Dannenberg, J. J.; Zakrzewski, V. G.; Dapprich, S.; Daniels, A. D.; Strain, M. C.; Farkas, O.; Malick, D. K.; Rabuck, A. D.; Raghavachari, K.; Foresman, J. B.; Ortiz, J. V.; Cui, Q.; Baboul, A. G.; Clifford, S.; Cioslowski, J.; Stefanov, B. B.; Liu, G.; Liashenko, A.; Piskorz, P.; Komaromi, I.; Martin, R. L.; Fox, D. J.; Keith, T.; Al-Laham, M. A.; Peng, C. Y.; Nanayakkara, A.; Challacombe, M.; Gill, P. M. W.; Johnson, B.; Chen, W.; Wong, M. W.; Gonzalez, C.; Pople, J. A. *Gaussian 03*, revision E.01; Gaussian, Inc.: Wallingford, CT, 2004.

(10) (a) Parr, R. G.; Yang, W. *Density Functional Theory of atoms and molecules*; Oxford University Press: Oxford, U.K., 1989; (b) Salahub, D. R.; Zerner, M. C. *The Challenge of d and f Electrons*; ACS Symposium Series 394; American Chemical Society: Washington, DC, 1989; (c) Kohn, W.; Sham, L. *J. Phys. Rev.* **1965**, *140*, A1133−A1138. (d) Hohenberg, P.; Kohn, W. *Phys. Rev.* **1964**, *136*, B864−B871.

(11) (a) Stratmann, R. E.; Scuseria, G. E.; Frisch, M. *J. Chem. Phys.* **1998**, *109*, 8218−8224. (b) Casida, M. E.; Jamoroski, C.; Casida, K. C.; Salahub, D. R. *J. Chem. Phys.* **1998**, *108*, 4439−4449. (c) Bauernschmitt, R.; Haser, M.; Treutler, O.; Ahlrichs, R. *Chem. Phys. Lett.* **1996**, *256*, 454−464.

(12) (a) Becke, A. D. *J. Chem. Phys.* **1993**, *98*, 5648−5652. (b) Miehlich, B.; Savin, A.; Stoll, H.; Preuss, H. *Chem. Phys. Lett.* **1989**, *157*, 200−205. (c) Lee, C.; Yang, W.; Parr, R. G. *Phys. Rev. B* **1988**, *37*, 785−789.

(13) (a) Bruke, K.; Perdew, J. P.; Wang, Y. *Electronic Density Functional Theory: Recent Progress and New Direction*; Dobson, J. F., Vignale, G., Das, M. P., Eds.; Plenum: New York, 1998; (b) Perdew, J. P.; Bruke, K.; Wang, Y. *Phys. Rev.* **1996**, *B54*, 16533−16539. (c) Perdew, J. P.; Chevary, J. A.; Vosko, S. H.; Jackson, K. A.; Pederson, M. R.; Sing, D. J.; Fiolhais, C. *Phys. Rev.* **1993**, *B48*, 4978−4978. (d) Perdew, J. P.; Chevary, J. A.; Vosko, S. H.; Jackson, K. A.; Pederson, M. R.; Sing, D. J.; Fiolhais, C. *Phys. Rev.* **1992**, *B46*, 6671−6687. (e) Perdew, J. P. *Electronic Structure of Solids*, '91; Ziesche, P., Eschrig, H., Eds.; Akademie Verlag: Berlin, Germany, 1991.

(14) (a) Ernzerhof, M.; Scuseria, G. E. *J. Chem. Phys.* **1999**, *110*, 5029−5036. (b) Perdew, J. P.; Burke, K.; Ernzerhof, M. *Phys. Rev. Lett.* **1997**, *78*, 1396−1396. (c) Perdew, J. P.; Ernzerhof, M.; Burke, K. *J. Chem. Phys.* **1996**, *105*, 9982−9985. (d) Perdrew, J. P.; Burke, K.; Ernzerhof, M. *Phys. Rev. Lett.* **1996**, *77*, 3865−3868.

(15) Pulay, P. *J. Comput. Chem.* **1982**, *3*, 556−560.

(16) Schlegel, H. B.; McDouall, J. J. In *Computational Advances in Organic Chemistry*; Ogretir, C., Csizmadia, I. G., Eds.; Kluwer Academic: Dordrecht, The Netherlands, 1991; pp 167−185.

(17) (a) Hay, P. J.; Wadt, W. R. *J. Chem. Phys.* **1985**, *82*, 270−283. (b) Wadt, W. R.; Hay, P. J. *J. Chem. Phys.* **1985**, *82*, 284−298. (c) Hay, P. J.; Wadt, W. R. *J. Chem. Phys.* **1985**, *82*, 299−310.

(18) (a) Petersson, G. A.; Al-Laham, M. A. *J. Chem. Phys.* **1991**, *94*, 6081−6090. (b) Petersson, G. A.; Bennett, A.; Tensfeldt, T. G.; Al-Laham, M. A.; Shirley, W. A.; Mantzaris, J. *J. Chem. Phys.* **1988**, *89*, 2193−2218.

(19) (a) Rassolov, V. A.; Ratner, M. A.; Pople, J. A.; Redfern, P. C.; Curtiss, L. A. *J. Comput. Chem.* **2001**, *22*, 976−984. (b) Francl, M. M.; Pietro, W. J.; Hehre, W. J.; Binkley, J. S.; DeFrees, D. J.; Pople, J. A.; Gordon, M. S. *J. Chem. Phys.* **1982**, *77*, 3654−3665. (c) Hariharan, P. C.; Pople, J. A. *Mol. Phys.* **1974**, *27*, 209−214. (d) Hariharan, P. C.; Pople, J. A. *Theor. Chim. Acta.* **1973**, *28*, 213−222. (e) Hehre, W. J.; Ditchfield, R.; Pople, J. A. *J. Chem. Phys.* **1972**, *56*, 2257−2261.

(20) (a) Frisch, M. J.; Pople, J. A.; Binkley, J. S. *J. Chem. Phys.* **1984**, *80*, 3265−3269. (b) Clark, T.; Chandrasekhar, J.; Spitznagel, G. W.; Schleyer, P. V. R. *J. Comput. Chem.* **1983**, *4*, 294−301.

(21) Brown, S. N. *Inorg. Chem.* **2012**, *51*, 1251−1260.

(22) Consider the percentage (%) of $L^{R'}{}_{SQ}{}^{-\bullet}$ be *x* and the percentage (%) of $L^{R'}{}_{CAT}{}^{2-}$ be *y*, condition: $x + y = 100$, $x/100(-1) + y/100(-2) = MOS$.

(23) Scheffer, J. R.; Wong, Y. -F.; Patil, A. O.; Curtin, D. Y.; Paul, I. C. *J. Am. Chem. Soc.* **1985**, *107*, 4898−4904.

(24) Chatterjee, P. B.; Goncharov-Zapata, O.; Quinn, L. L.; Hou, G.; Hamaed, H.; Schurko, R. W.; Polenova, T.; Crans, D. C. *Inorg. Chem.* **2011**, *50*, 9794−9803.

(25) (a) Sanna, D.; Ugone, V.; Micera, G.; Garribba, E. *Dalton Trans.* **2012**, *41*, 7304−7318. (b) Maurya, M. R.; Bisht, M.; Kumar, A.; Kuznetsov, M. L.; Avecilla, F.; Pessoa, J. C. *Dalton Trans.* **2011**, *40*, 6968−6983. (c) Maurya, M. R. *J. Chem. Sci.* **2011**, *123*, 215−228. (d) Ramos, S.; Rui O. Duarte, R. O.; Mourac, J. J. G.; Aureliano, M. *Dalton Trans.* **2009**, 7985−7994. (e) Maurya, M. R.; Arya, A.; Kumar, A.; Pessoa, J. C. *Dalton Trans.* **2009**, 2185−2195. (f) Rangel, M.; Leite, A.; Amorim, M. J. *Inorg. Chem.* **2006**, *45*, 8086−8097. (g) Gätjens, J.; Meier, B.; Adachi, Y.; Sakurai, H.; Rehder, D. *Eur. J. Inorg. Chem.* **2006**, 3575−3585. (h) Maurya, M. R.; Kumar, A.; Ebel, M.; Rehder, D. *Inorg. Chem.* **2006**, *45*, 5924−5937. (i) Smith, T. S., II; Root, C. A.; Kampf, J. W.; Rasmussen, P. G.; Pecoraro, V. L. *J. Am. Chem. Soc.* **2000**, *122*, 767−775.

(26) Kubelka, P.; Munk, F. *Z. Tech. Phys.* **1931**, *12*, 593−601.

(27) Pierpont, C. G. *Coord. Chem. Rev.* **2001**, *216*−*217*, 99−125.

(28) (a) Attia, A. S.; Pierpont, C. G. *Inorg. Chem.* **1995**, *34*, 1172−1179. (b) Attia, A. S.; Pierpont, C. G. *Inorg. Chem.* **1997**, *36*, 6184−6187.

(29) Rehder, D. *Coord. Chem. Rev.* **2008**, *252*, 2209−2223.